ELSEVIER

Journal of Structural Geology 27 (2005) 1379–1398

JOURNAL OF STRUCTURAL GEOLOGY

www.elsevier.com/locate/jsg

$^{40}Ar/^{39}Ar$ dating of strike-slip motion on the Tan–Lu fault zone, East China

Guang Zhu*, Yongsheng Wang, Guosheng Liu, Manlan Niu, Chenglong Xie, Changcheng Li

Department of Geology, School of Resource and Environment Engineering, Hefei University of Technology, Tunxi Road 193, Hefei, Anhui Province 230009, People's Republic of China

Received 1 November 2004
Available online 6 July 2005

Abstract

NE-trending, sinistral ductile shear belts in the southern part of the Tan–Lu fault zone, East China are exposed along the eastern edge of the northern Dabie belt and southern Zhangbaling belt. Three hornblende, three phengite and 12 biotite separates from greenschist facies mylonites in the shear belts were dated by the $^{40}Ar/^{39}Ar$ method in this study. A hornblende plateau age of 143.3 Ma is interpreted as representing the time of sinistral motion on the Zhangbaling part of the Tan–Lu fault zone. Seven biotite samples from the same part yield $^{40}Ar/^{39}Ar$ cooling ages from 137 to 125 Ma. A phengite plateau age of 138.8 Ma from the eastern edge of the Dabie belt is considered as being close to the time of deformation in the Tan–Lu strike-slip zone. Five biotite $^{40}Ar/^{39}Ar$ ages from 120 to 110 Ma and one phengite age of 121 Ma from the same area represent cooling ages after the sinistral faulting. It is concluded on the basis of these $^{40}Ar/^{39}Ar$ ages that the sinistral ductile shear belts in the southern part of the Tan–Lu fault zone were produced in earliest Early Cretaceous. This sinistral motion on the Tan–Lu fault zone is considered to be related to high-speed, highly oblique subduction of the Pacific plate at this time.

Keywords: Tan–Lu fault zone; Mylonite; Dabie orogenic belt; Zhangbaling belt; $^{40}Ar/^{39}Ar$ dating; Early Cretaceous

1. Introduction

The NE–NNE striking Tan–Lu fault, with a length of 2400 km, is the largest fault zone in East China. It plays a key role in Mesozoic tectonic evolution of the East Asian continent (Xu et al., 1987). The fault zone sinistrally offsets the Dabie and Sulu orogenic belts between the North China Block (NCB) and South China Block (SCB), and about 550 km apparent displacement is shown by the northern boundary of the Dabie and Sulu orogenic belts (Fig. 1). Timing and mechanism of the offsetting remains controversial. Some workers proposed that the fault zone was a result of the NCB–SCB collision in Late Triassic (Indosinian movement). Syn-collisional models that have been proposed include the transform fault model (Zhang et al., 1984; Hsu et al., 1987; Okay and Sengor, 1992; Wan and Zhu, 1996; Wang et al., 1998), the indentation boundary model (Yin and Nie, 1993), the rotated suture line model (Lin and Fuller, 1990; Zhang, 1997; Gilder et al., 1999), the detachment/tear fault model (Li, 1994; Lin, 1995; Chung, 1999) and hinge fault model (Chang, 1996), while Lin (1995) attributed the detachment/tear faulting of Li (1994) to the indentation of Yin and Nie (1993). In contrast, Xu and Zhu (1994) pointed out that the fault zone did not exist during the NCB–SCB collision, but was initiated as a continental-scale strike-slip fault in the Late Jurassic to Early Cretaceous due to oblique subduction of the Pacific Izanagi plate beneath the East Asian continent.

Whether or not, and when, the fault zone experienced large-scale, sinistral movement after the NCB–SCB collision is also a subject of debate. Wan and Zhu (1996) denied any sinistral movement along the fault zone after the collision. Wang et al. (1998) argued that the fault zone experienced sinistral movement in the Jurassic. Lin et al. (1998) described foliated cataclastic rocks from the middle part of the fault zone (in the Shandong region) and argued that the sinistral faulting took place from the Cretaceous to the end of the Tertiary. Hong and Miyata (1999) studied the Mazhan basin along the middle part of the Tan–Lu fault and concluded that it was a pull-apart basin related to sinistral

* Corresponding author. Tel.: +86 551 2901524; fax: +86 551 2904517.
E-mail address: zhuguang@mail.hf.ah.cn (G. Zhu).

0191-8141/$ - see front matter © 2005 Elsevier Ltd. All rights reserved.
doi:10.1016/j.jsg.2005.04.007

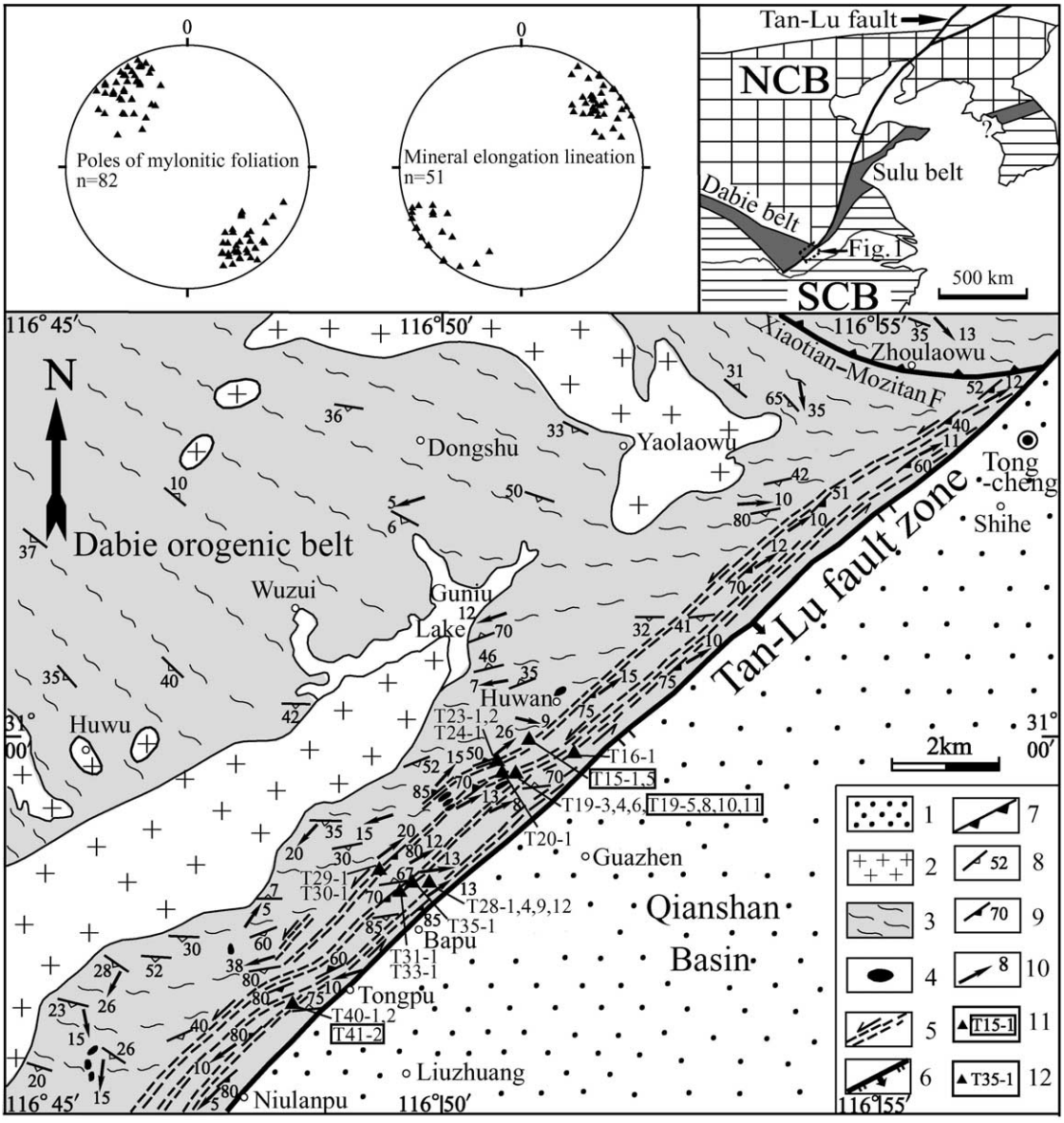

Fig. 1. Structural map of the Tongcheng–Niulanpu part of the Tan–Lu fault zone along the eastern edge of the Dabie orogenic belt. 1: Upper Cretaceous–Paleogene basin deposits; 2: Early Cretaceous intrusion; 3: gneissosity in Dabie metamorphic complexes; 4: eclogite; 5: ductile shear belt; 6: brittle normal fault; 7: main thrust; 8: attitude of gneissosity; 9: attitude of mylonitic foliation; 10: attitude of mineral elongation lineation; 11: sampling locality for $^{40}Ar/^{39}Ar$ dating; 12: sampling locality for quartz *c*-axis fabric analysis.

motion along its NNE-trending bounding faults. The basin was believed to be Late Cretaceous in age, but more recent studies have demonstrated that it is Early Cretaceous in age instead (Zhang et al., 2003). Zhou et al. (1999) also documented a Lower Cretaceous pull-part basin, the Shichang–Zhonglou basin, along the middle (Shandong) part of the fault zone. Based on fault-slip data from the Dabie orogenic belt, Ratschbacher et al. (2000) inferred that the Tan–Lu fault zone at the eastern edge of the Dabie belt was mainly a normal fault with an early sinistral and late dextral component. Thermochronological data indicate that the movement on the fault zone in this area took place in the Early Cretaceous. During the Late Cretaceous to Paleogene, the fault zone was involved in intense normal faulting that resulted in the development of the Qianshan Basin to the east of the Dabie belt (Ratschbacher et al., 2000; Grimmer et al., 2002). Based on field analysis of fault-slip data along the middle part of the fault zone, Zhang et al. (2003) recorded that the fault zone experienced dextral, normal and sinistral faulting from an earlier to a later stage of the Early Cretaceous. It is evident from the above review that the timing of sinistral movement on the Tan–Lu fault zone is an unsolved key problem. It concerns not only the evolution of the fault zone itself, but also the sequence of the collision of the NCB with SCB and the tectonic evolution of East Asia.

Reliable isotopic geochronological data for strike-slip

motion along the Tan–Lu fault zone were not available previously. Chen et al. (1989) reported K–Ar ages of 90–110 Ma for fine-grained (<1 μm) clays from a fault gouge in the middle part of the fault zone. However, Lin et al. (1998) attributed the fault gouge to Quaternary dip-slip faulting, which renders the geological significance of these K–Ar ages uncertain. Zhu et al. (1995) obtained five K–Ar whole-rock ages of 103–95 Ma from mylonites in the sinistral ductile shear belts in the Zhangbaling part (Anhui region) of the fault zone and interpreted them as cooling ages related to the strike-slip motion. More recently, Zhu et al. (2001a) reported six $^{40}Ar/^{39}Ar$ whole-rock plateau ages of 132–120 Ma from a mylonite, ultramylonite and phyllonite in the sinistral shear belts in the southern part of the Tan–Lu fault zone. Considering that the powdered material used in the whole-rock analyses contain various K-bearing minerals with different closure temperatures, these K–Ar and $^{40}Ar/^{39}Ar$ whole-rock ages only give mixing ages that are different from the cooling or deformation ages. In this context, $^{40}Ar/^{39}Ar$ dating performed in this study was done on biotite, white mica and hornblende mineral separates from mylonites in sinistral shear belts in the southern part of the Tan–Lu fault zone. The new $^{40}Ar/^{39}Ar$ ages offer reliable information about timing of the Tan–Lu strike-slip motion and bear important tectonic implications.

2. Ductile shear belts

The southern part of the Tan–Lu fault zone is situated along the eastern edge of the Dabie orogenic belt in the south and the Zhangbaling belt in the north (Fig. 1). The main rock units in the Dabie belt, from south to north, are the high-pressure (HP) blueschist, HP amphibolite, HP quartz eclogite and ultra-high pressure (UHP) coesite eclogite. Further to the north is the Northern Orthogneiss unit with Early Cretaceous intrusions and the Luzhengguang and Fuziling groups to the north of the Xiaotian–Mozitang fault zone (Hacker et al., 2000; Faure et al., 2003). Triassic to Early Jurassic metamorphic ages have been well documented in the Dabie belt (Hacker et al., 2000). Sinistral offsetting of the Dabie and Sulu orogenic belts by the Tan–Lu fault zone produced a NNE-trending tectonic slice, the Zhangbaling belt that includes metamorphic complexes known as the Feidong and Zhangbaling groups, between the two orogenic belts (Fig. 2). The northern part of the Zhangbaling belt includes the low-grade Zhangbaling Group, whereas the southern part contains the high-grade Feidong Group (without reliable isotopic ages) with local exposures of the Zhangbaling Group on its eastern and southern margins. The occurrence of HP blueschist with Triassic isotopic ages (Li et al., 1993) in the Zhangbaling group indicates that the Zhangbaling belt was a part of the Dabie–Sulu orogenic belt before the sinistral offset. The Hefei Basin filled with Jurassic to Paleogene strata (Zhu et al., 2001b) overlies the NCB and occurs to the west of the Zhangbaling belt, whereas the Lower Yangtze foreland fold and thrust belt, related to the NSB–SCB collision, is present to the east of the belt (Fig. 2).

2.1. The eastern edge of the Dabie orogenic belt

Strike-slip structures in the Tan–Lu fault zone at the eastern edge of the Dabie orogenic belts occur as large-scale ductile shear belts. Owing to later overlap of the Qianshan Basin filled with Upper Cretaceous to Paleogene strata (Zhu et al., 2001b), the ductile shear belts are primarily exposed from Tongcheng to Niulanpu (Fig. 1), along the eastern margin of the Northern Orthogneiss Unit of the Dabie belt. Normal faults related to the development of the Qianshan Basin are observed to truncate the eastern edge of the ductile shear zone (Fig. 1).

Strike-slip structures exposed in the Tongcheng–Niulanpu part of the Tan–Lu fault zone include several ductile shear belts within a ca. 2-km-wide zone. Towards the shear belts, gneissic foliation in the Dabie metamorphic complexes generally changes its strikes from NW to ENE to NE, as a result of sinistral motion along the fault zone (Fig. 1). Fieldwork demonstrates that 2–4 main shear belts, with widths of tens to a few hundreds of metres, are present in this part of the fault zone. Each of the shear belts is characterized by the presence of protomylonite, mylonite and local ultramylonite (Fig. 3a–c; Sibson, 1977). Between the main shear belts, NEE-striking foliation of the gneisses are preserved. Foliation in the orogenic gneisses is cut by and curved into the NE-striking shear belts. The shear belts strike N45°E in general. The mylonitic foliation in the belts dips steeply and stretching lineation defined by elongated quartz grains on the foliation plunge shallowly to subhorizontally (Fig. 1). The lineation plunges northeastly to the north of Bapu and southwestly to the south. S–C fabrics, rotated feldspar porphyroblasts and the curvature of pre-existing foliations all indicate sinistral shear sense. It is evident that the NE-striking ductile shear belts in the Tan–Lu fault on the eastern edge of the Dabie orogenic belt zone were a result of sinistral motion.

2.2. The southern Zhangbaling belt

Field work shows that NE-striking, discrete ductile shear belts also occur in the southern Zhangbaling belt, overprinting the metamorphic complexes (Fig. 2). In a ca. 5-km-wide area within the northern part of the southern Zhangbaling belt, 6–8 shear belts are recognized (Fig. 2), with widths varying from tens of metres to ca. 300 m. Protomylonite, mylonite and local ultramylonite (Fig. 3d–f) occur in each of the shear belts. The mylonitic foliation in the shear belts in the northern part dominantly strikes N35°E and dips 65°–80°SE (Fig. 2). The mineral elongation lineation on the mylonitic foliation predominantly plunges shallowly 10–20°SW (Fig. 2). In the southern part of the southern Zhangbaling belt, there are five discrete ductile

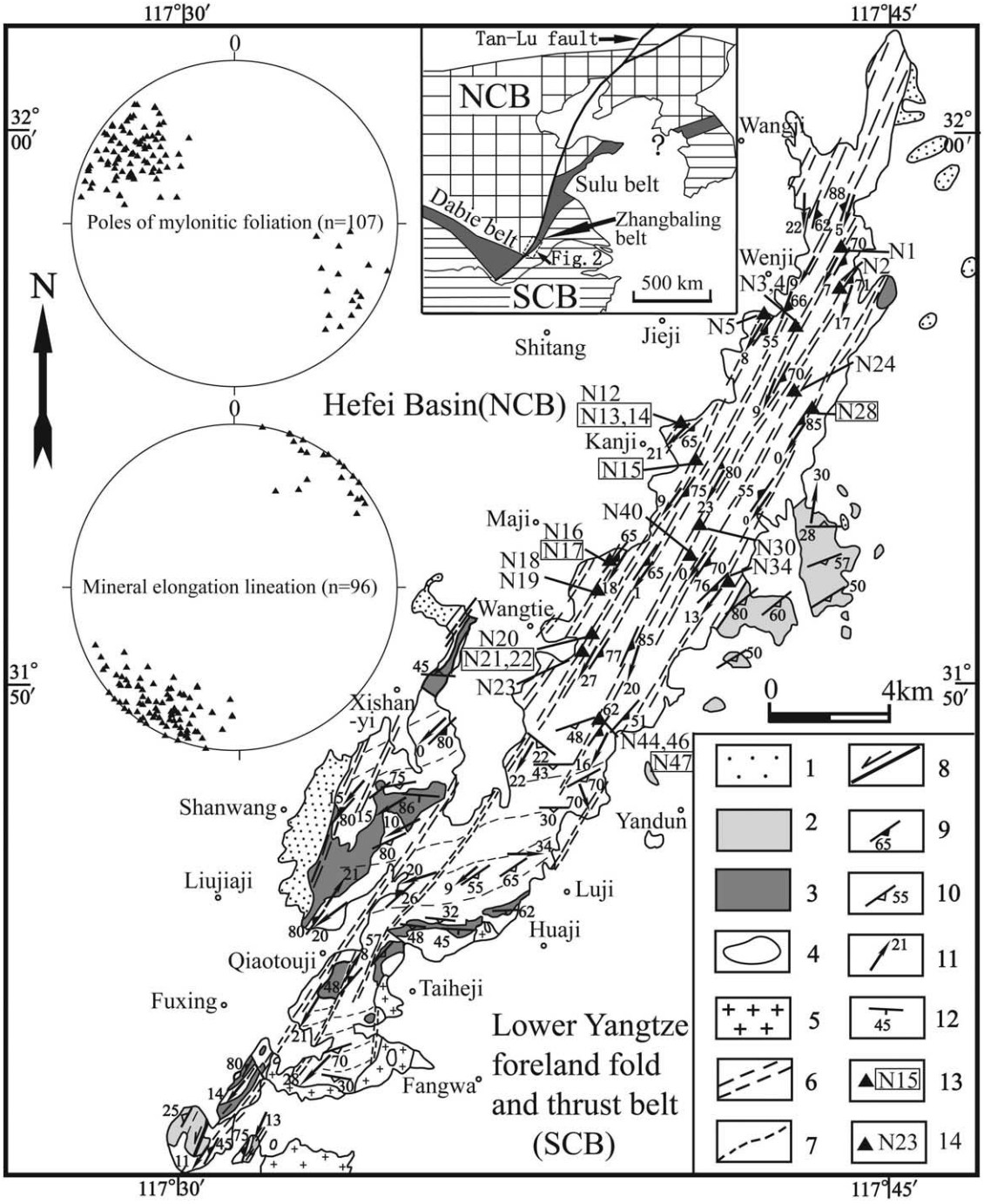

Fig. 2. Structural map of the southern Zhangbaling belt. 1: Upper Cretaceous basin deposits; 2: Late Proterozoic rocks (Zhangbaling group) containing blueschists; 3: marble in the Feidong Group; 4: gneisses in the Feidong Group; 5: Early Cretaceous intrusion; 6: ductile shear belts; 7: trace of metamorphic foliation; 8: brittle fault; 9: attitude of mylonitic foliation; 10: attitude of metamorphic foliation; 11: attitude of mineral elongation lineation; 12: attitude of strata; 13: sampling locality for $^{40}Ar/^{39}Ar$ dating; 14: Sampling locality for quartz *C*-axis fabric analysis.

shear belts (Fig. 2), each of them a few to tens of metres in width, indicating that ductile deformation here is weaker than that in the northern part. Between the shear belts, the pre-existing metamorphic foliation strikes ENE in general and curves into the NE direction towards the shear belts. The metamorphic foliation curvature indicates the sinistral shear sense along the shear belts (Fig. 2). S–C fabrics and rotated feldspar porphyroblasts also indicate sinistral shear sense.

3. Microfabric and sample descriptions

To determine the shear sense and estimate the

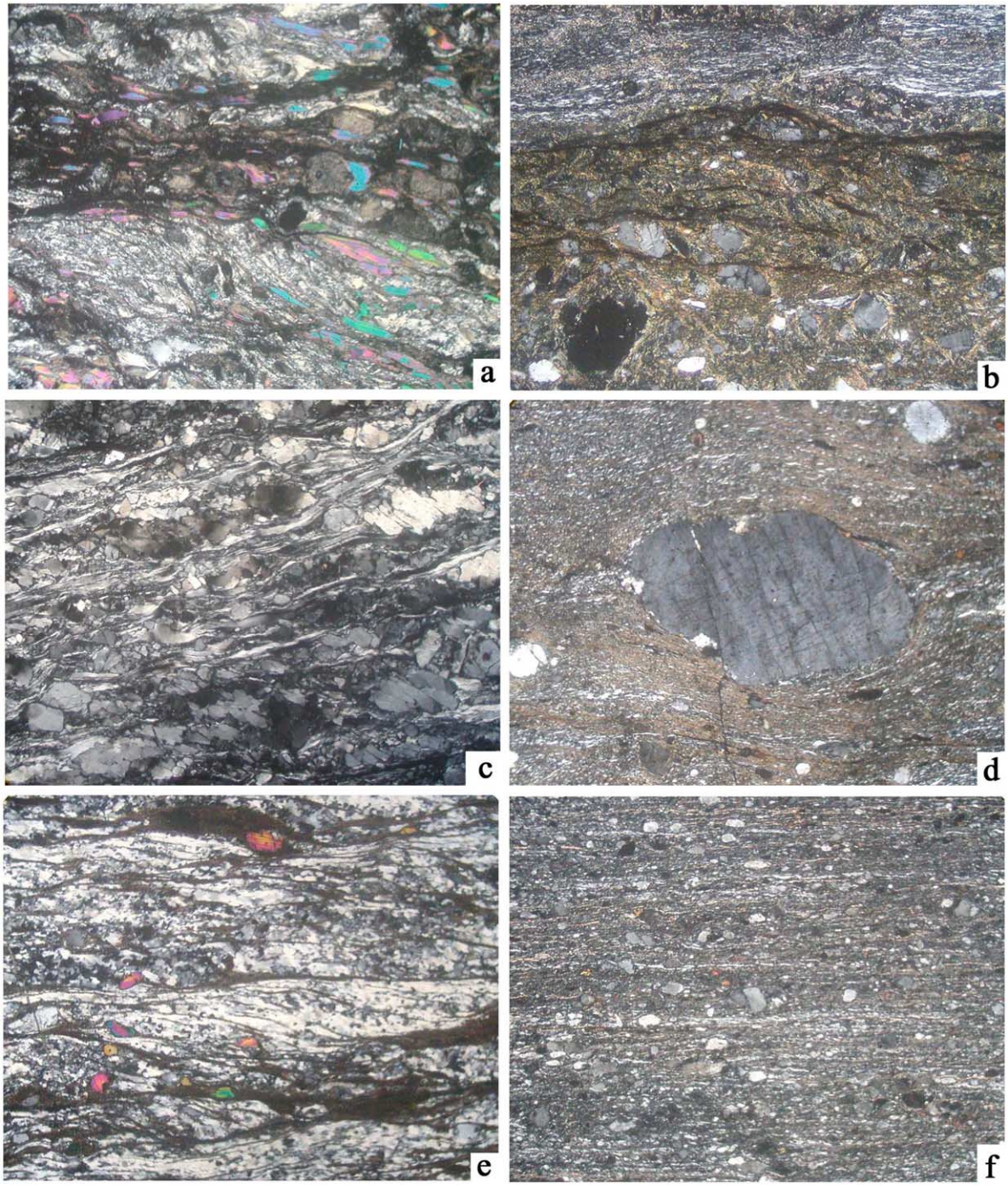

Fig. 3. Photomicrographs of mylonites from the southern part of the Tan–Lu fault zone. All thin-sections parallel with *XZ* plane. Width of view is 4 mm, except for (b), which is 1.6 mm. Crossed polarizers. Sample localities are shown in Figs. 1 and 2. (a) White mica-bearing mylonite T15-5, showing widespread dynamic recrystallization of quartz and elongated porphyroclastic feldspar with muscovitisation. Oblique foliation defined by muscovite and quartz, as well as mica fish, indicates sinistral shear sense. (b) Biotite-bearing mylonite T19-5. Porphyroclasts are feldspar and biotite. The matrix is dominated by fine-grained biotite and recrystallized quartz. S–C fabrics defined by biotite show sinistral shear sense. (c) Protomylonite T28-9 with intensely elongated quartz ribbon. 'Book-shelf' fractured feldspar shows sinistral shear sense. (d) Biotite-bearing ultramylonite N2. The matrix is composed of recrystallized quartz, fine biotite and feldspar. A σ-type feldspar porphyroclast surrounded by dynamically recrystallized feldspar indicates sinistral shear sense. (e) Biotite-bearing ultramylonite N30. The matrix is dominated by fine biotite, recrystallized quartz and epidote. S–C fabrics defined by biotite and recrystallized quartz indicate sinistral shear sense. (f) Ultramylonite N45. The matrix is composed of fine biotite, fractured feldspar and recrystallized quartz. Local 'book-shelf' fractured feldspar indicates sinistral shear sense.

deformation temperature of the Tan–Lu ductile shear belts, we collected oriented mylonite samples from the eastern edge of the Dabie belt and southern part of the Zhangbaling belt (Figs. 1 and 2). Microscopic study of 35 oriented thin-sections cut parallel with the *XZ* plane of the finite strain ellipsoid from the Dabie belt and 37 thin-sections from the Zhangbaling belt further demonstrates sinistral shear sense of the shear belts. Shear sense indicators observed include mica-fish, S–C fabrics, 'book-shelf' structures and rotated feldspar porphyroclasts (Fig. 3a–e).

The orientation of C-axis of dynamically recrystallized quartz in the mylonites was measured using a U-stage and the results are shown in Figs. 4 and 5 (plotted using StereoNett 2.46). Their asymmetry with respect to foliation (*XY* plane) also indicates sinistral sense of shear. The lattice-preferred orientation (LPO) patterns are dominated by near-periphery, double point maximum patterns, indicating activities of dominant basal plane slip with some rhomb plane slip in the dynamically recrystallized quartz during the mylonization (Passchier and Trouw, 1996). A few of the samples (e.g. T19-3, T-19-4, T19-6 and T40-2 from the eastern edge of the Dabie belt (Fig. 4) and N1, N2, N3, N12 and N14 (Fig. 5) from the southern Zhangbaling belt) show central girdles or type I crossed girdles, indicating coeval basal, rhomb and prism plane slip. All of the LPO patterns suggest that the mylonites were developed under low-grade conditions (Passchier and Trouw, 1996), which is consistent with the results of temperature estimates presented below.

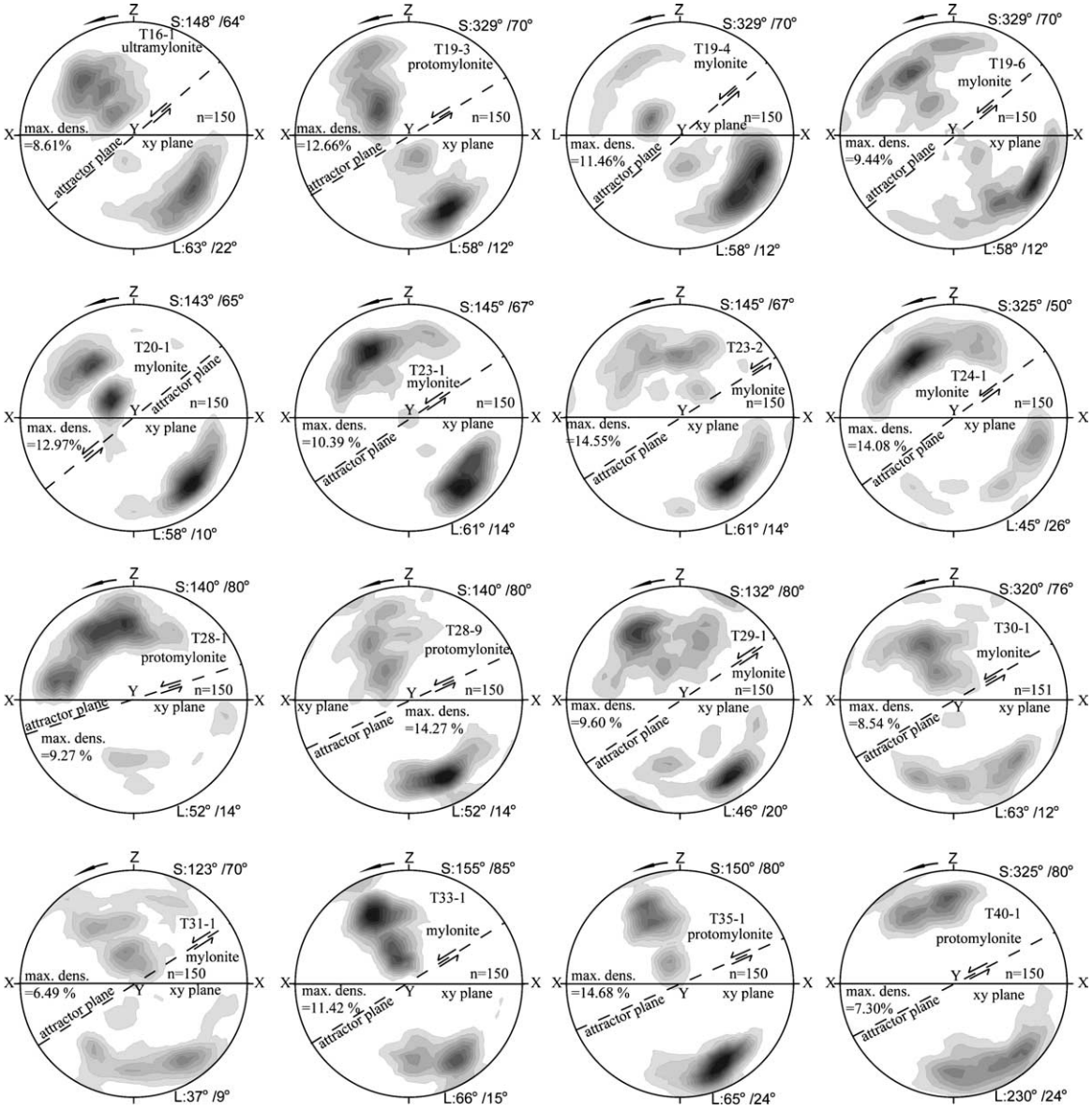

Fig. 4. *C*-axis fabric stereograms of dynamic recrystallisation quartz in mylonites from the Tan–Lu fault zone at the eastern edge of the Dabie orogenic belt. Contours are 1, 2, up to 14% per 1% area. Lower-hemisphere, equal-area projection. The thin-sections are parallel with *XZ* plane. *X*,*Y*, *X* are principle axes of finite strain. *S*: mylonitic foliation attitude (dip direction/dip angle); *L*: mineral elongation lineation attitude (plunge direction/plunge angle). *n*: measured grain numbers.

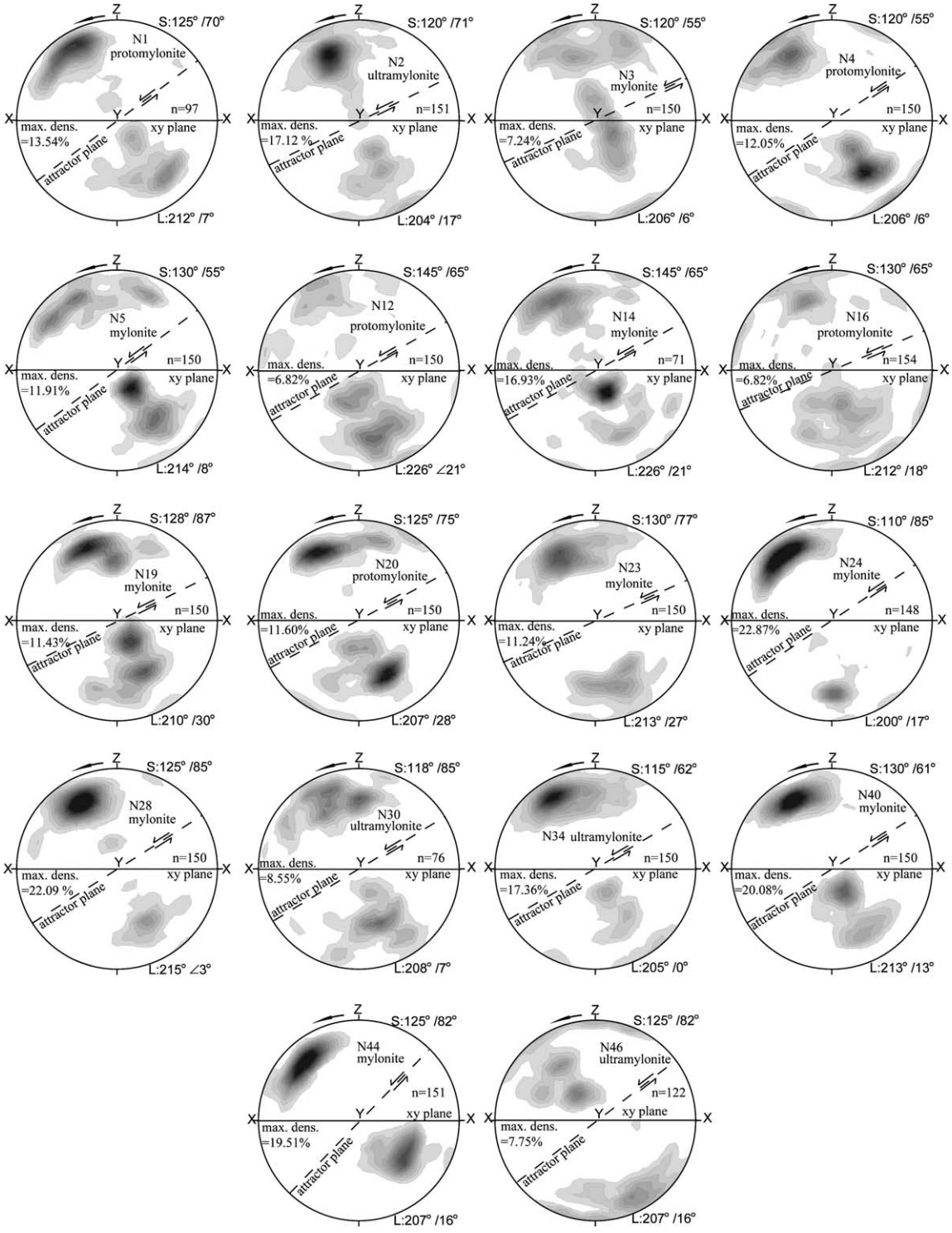

Fig. 5. C-axis fabric stereograms of dynamic recrystallisation quartz in mylonites from the southern Zhangbaling part of the Tan–Lu fault zone. Contours are 1, 2 up to 22% per 1% area. Lower-hemisphere, equal-area projection. The thin-sections are parallel with *XZ* plane. *X*,*Y*, *X* are principle axes of finite strain. *S*: mylonitic foliation attitude (dip direction/dip angle); *L*: mineral elongation lineation attitude (plunge direction/plunge angle). *n*: measured grain numbers.

Monoclinic symmetry predominates in the LPO, indicating dominant non-coaxial deformation in the mylonites (Passchier and Trouw, 1996).

Seven mylonite samples from three localities in the ductile shear belts at the eastern edge of the Dabie belt and 10 mylonite samples from seven localities in the southern Zhangbaling belt were collected (Figs. 1 and 2) for dating in this study. Descriptions of the samples, based on microscopic observation, are given in Table 1. The dated samples are mylonite or protomylonite. Their porphyroclasts are

Table 1
Descriptions of the dated mylonites in the Tan–Lu ductile shear belts

Sample	Locality	Rock type	Assemblage	Si in white mica (pfu)	Feldspar deformation	Quartz recystallisation	Estimated T (°C)
T15-1	Hushanzui: 30°59′49.2″N; 116°51′00.0″E	Protomylonite	P (65%): Fel + Qz + Bi + Phe; M (35%): Qz + Bi + Chl + Ep	P: 3.36; M: 3.20	Fracturing and elongated	SR	ca. 400
T15-5	Hushanzui: 30°58′26.1″N; 116°49′39.7″E	Protomylonite	P (75%): Fel + Qz + Phe; M (25%): Qz + Mus + Chl	P: 3.36, 3.37'; M: 3.19	Elongated	SR + GBM	400–450
T19-5	Chengban: 30°59′23.3″N; 116°51′09.0″E	Mylonite	P (40%): Fel + Bi; M (60%): Qz + Bi + Chl + Ep		Fracturing and elongated	SR	ca. 400
T19-8	Chengban: 30°59′23.3″N; 116°51′09.0″E	Mylonite	P (35%): Fel + Bi; M (65%): Qz + Bi + Ep		Fracturing and elongated	SR	ca. 400
T19-10	Chengban: 30°59′23.3″N; 116°51′09.0″E	Mylonite	P (30%): Fel + Bi; M (70%): Qz + Bi + Chl + Ep		Fracturing and elongated	SR	ca. 400
T19-11	Chengban: 30°57′15.8″N; 116°51′09.0″E	Protomylonite	P (60%): Fel + Qz + Phe + Bi; M (40%): Qz + Mus + Bi + Chl + Ep	P: 3.35, 3.36	Fracturing and elongated	SR + GBM	ca. 400
T41-2	Citangkou: 30°59′23.3″N; 116°48′29.0″E	Mylonite	P (45%): Fel + Mus; M (55%):Fel + Qz + Mus + Chl + Ep		Dominantly recrystallised	SR + GBM	500–550
N13	Miaoshan: 31°54′35.7″N; 117°40′33.8″E	Mylonite	P (30%): Qz + Fel + Hb; M (70%): Qz + Bi + Fel		Elongated and partially recrystallised	SR + GBM	ca. 500
N14	Miaoshan: 31°54′35.7″N; 117°40′33.8″E	Mylonite	P (20%): Fel + Hb + Qz; M (80%): Bi + Fel + Qz + Fel		Elongated and partially recrystallised	SR + GBM	ca. 500
N15	Eastern Kanji: 31°53′53.5N″; 117°40′51.6″E	Mylonite	P (30%): Fel + Qz + Bi; M (70%): Qz + Bi + Fel		Elongated and partially recrystallised	SR + GBM	ca. 500
N17	Wangshanwei: 31°52′12.3″N; 117°39′15.0″E	Mylonite	P (50%): Qz + Fel + Bi; M (50%): Qz + Bi + Fel		Elongated and partially recrystallised	SR + GBM	ca. 500
N18	Gongchao: 31°51′29.1″N; 117°38′56.2″E	Mylonite	P (20%): Fel + Qz + Hb; M (80%): Bi + Qz		Elongated	SR + GBM	ca. 450
N21	Songshanwa: 31°50′52.7″N; 117°38′54.5″E	Protomylonite	P (80%): Fel + Qz + Bi; M (20%): Qz + Bi + Ep		Elongated	SR + GBM	ca. 450
N22	Songshanwa: 31°50′52.7″N; 117°38′54.5″E	Protomylonite	P (75%): Qz + Fel + Bi; M (25%): Qz + Bi + Ep		Elongated	SR + GBM	ca. 450
N28	Yantoushan: 31°54′35.3″N; 117°42′56.3″E	Mylonite	P (30%): Hb + Fel + Qz; M (70%): Bi + Qz + Ep		Elongated	SR + GBM	ca. 450
N47	Xiwei: 31°49′06.6″N; 117°38′28.8″E	Protomylonite	P (75%): Fel + Hb + Qz + Bi; M (25%): Qz + Bi + Ep		Elongated	SR + GBM	ca. 450

Qz: quartz; Fel: feldspar; Bi: biotite; Mus: muscovite; Phe: phengite; Chl: chlorite; Ep: epidote; P: porphyroclast; M: matrix; SR: subgrain rotation recrystallisation; GBM: grain boundary migration recrystallization; error for the estimated temperature is less than 50 °C.

feldspars (plagioclase and/or K-feldspar), elongated quartz, white mica, biotite or hornblende (Fig. 3). The porphyroclasts are preferentially oriented along foliation. Four types of deformation can be found in the feldspars: fracturing with partial elongation, elongation, elongation with partial recrystallization and dominant recrystallization (Table 1). The matrices are fine-grained, recrystallized quartz, muscovite, biotite, chlorite or epidote (Table 1; Fig. 3). Their grain widths are mostly less than 20 μm. In the matrices, quartz shows evidence for subgrain rotation (SR) recrystallisation and grain boundary migration (GBM) recrystallisation in most samples, except for samples T15-1, T19-5, T19-8 and T19-10, in which only evidence for SR recrystallization is observed (Table 1).

4. Estimates of P–T conditions

To determine pressure conditions experienced by the ductile shear belts, we conducted electron microprobe analysis on white mica in five mylonite samples from the eastern edge of the Dabie orogenic belt. The analysis was undertaken at the Electron Microprobe Laboratory, Testing Center, China University of Geosciences, using a JCXA-733 Electron microprobe. Porphyroclasts of white mica in all analyzed samples have Si atoms (per 11 oxygen) of >3.3 pfu (T28-4: 3.38, 3.39 pfu; T28-12: 3.45, 3.48 pfu; T15-1:3.36 pfu; T15-5:3.36, 3.37 pfu; T19-11: 3.35, 3.36 pfu), and are therefore medium- to high-Si phengite related to HP metamorphism during the Dabie orogeny.

These data show that the Tan–Lu fault zone overprints HP rocks of the Dabie belt. These results also demonstrate that the prophyroclastic white mica separates (T15-5, T19-11 and T41-2) dated in this study are phengite. On the other hand, syn-mylonization white mica in the matrices of the analyzed mylonites is all low-Si muscovite with Si atoms of <3.22 pfu (T28-4: 3.19 pfu; T28-12: 3.22 pfu; T15-1: 3.20 pfu; T15-5: 3.19 pfu). This suggests that the mylonites in the Tan–Lu ductile shear belts at the eastern edge of the Dabie belt were produced under low-pressure conditions. These results imply that the Tan–Lu ductile shear belts were formed after the Late Triassic HP metamorphism of the Dabie orogenic belt (Hacker et al., 2000).

Syn-mylonization mineral assemblages and mineral deformation behaviour in mylonites are closely related to deformation temperatures and can therefore be used to estimate deformation temperatures. The mineral assemblages observed in the matrices of the dated mylonite (see Table 1), especially the presence of biotite, indicate middle greenschist facies conditions. Greenschist facies temperatures range from 300 to 500 °C (Essene, 1989), and middle greenschist facies conditions range from 400 to 450 °C. Studies by Urai et al (1986) and Mancktelow and Pennacchioni (2004) show that with increasing temperatures SR recrystallisation transfers into GBM recrystallisation in quartz, with the transition taking place at ca. 400 °C. SR and GBM recrystallisation coexists between 400 and 700 °C. The dated samples contain evidence for both SR and GBM recrystallisation of quartz, except for samples T15-1, T19-5, 8 and 10, in which only evidence for SR recrystallization is present. Passchier and Trouw (1996) pointed out that feldspars show brittle fracturing at temperatures <400 °C; plastic elongation, undulose extinction, subgrains and core-mantle structure between 400 and 500 °C and dynamic recrystallisation dominates over 500 °C. Based on these temperature indicators, deformation temperatures for the dated mylonites are estimated and the results are summarized in Table 1. Errors for the estimated temperatures should be less than 50 °C. With the exception of sample T41-2 that experienced a temperature of 500–550 °C, the dated mylonites were developed under middle to upper greenschist facies conditions with temperatures of ca. 400, 450–500 and ca. 500 °C, respectively.

5. $^{40}Ar/^{39}Ar$ analytical results

Three white mica and five biotite samples from the eastern edge of the Dabie belt and seven biotite and three hornblende samples from the southern Zhangbaling belt were separated by means of standard separation techniques for $^{40}Ar/^{39}Ar$ dating. On the basis of microscopic observation, size fractions of >100 μm were chosen to obtain porphyroclasts of white mica and hornblende, and >85 μm was chosen for porphyroclastic or matrix biotite. The matrix micas in the mylonite samples mostly have widths of a few micrometers. They have quite low closure temperatures (Reddy and Potts, 1999) and are thus not suitable for dating deformation. They are also too fine-grained to be separated from the mylonites. Therefore, most dated minerals are the porphyroclasts from the mylonites. The only two exceptions are samples N13 and N14 in which biotite occurs only as a syn-mylonization mineral in matrices and has grain sizes of 40–120 μm.

The minerals were irradiated in the H8 position of the Swimming Pool Reactor at the Institute of Atomic Energy, Chinese Academy of Sciences, Beijing. The monitor used in this study is the Fangshan standard biotite (ZBH-25) with an age of 132.7 ± 1.2 Ma and potassium content of 7.6%. $^{40}Ar/^{39}Ar$ analyses of the samples from the eastern edge of the Dabie belt were conducted with an MM-1200B mass spectrometer at the Ar–Ar Laboratory, Institute of Geology, Chinese Academy of Geological Sciences, Beijing. The machine conditions and analytical methodology were described by Zhang et al. (2004). The analyses for the samples from the Zhangbaling belt were conducted with an MM5400 mass spectrometer at the Ar–Ar Laboratory, Institute of Geology and Geophysics, Chinese Academy of Sciences, Beijing. The analytical methods are summarized in Li et al. (2003).

The decay constant used is $\lambda=5.543\times10^{-10}\,a^{-1}$. The $^{40}Ar/^{39}Ar$ analytical data are listed in the Appendix. Age spectra and inverse isochrones (proceeded by using program ISOPLOTS2.49; Ludwig, 2001) are plotted in Figs. 6 and 7. The plateau ages were defined and calculated by using the program ISOPLOTS2.49 (Ludwig, 2001). All errors are quoted at the 1σ level.

5.1. The eastern edge of the Dabie orogenic belt

One phengite (T15-5) and one biotite (T15-1) separate from the same quarry were dated in this study. $^{40}Ar/^{39}Ar$ plateau ages (Tp) were obtained from the phengite T15-5 (138.8 ± 0.4 Ma) and the biotite T15-1 (110.7 ± 0.2 Ma), respectively. The plateau ages agree with their total gas ages (TGA) and inverse isochron ages (Ti) within errors (Fig. 6). The two plateau ages are accepted for later geological interpretation.

Four biotite samples from one quarry yield plateau ages of 119.9 ± 0.2 Ma (T19-11), 119.7 ± 0.4 Ma (T19-10), 117.6 ± 0.2 Ma (T19-5), and 109.8 ± 0.2 Ma (T19-8). The plateau ages closely agree with their TGA and T_i (Fig. 6) and are considered to be geologically meaningful. Another phengite sample, T19-11, from the same quarry does not give a plateau age (Fig. 6). Its variable age spectra are indicative of partial resetting. A weighted mean age (WMA) of the phengite for higher temperature steps is 192.6 ± 1.1 Ma (12–18 steps and 57% of cumulative ^{39}Ar release). This age is similar to the $^{40}Ar/^{39}Ar$ phengite ages of 195–190 Ma obtained by Hacker et al. (2000) from the UHP eclogite zone in the southern Dabie belt, which were interpreted as cooling ages related to early exhumation. It is

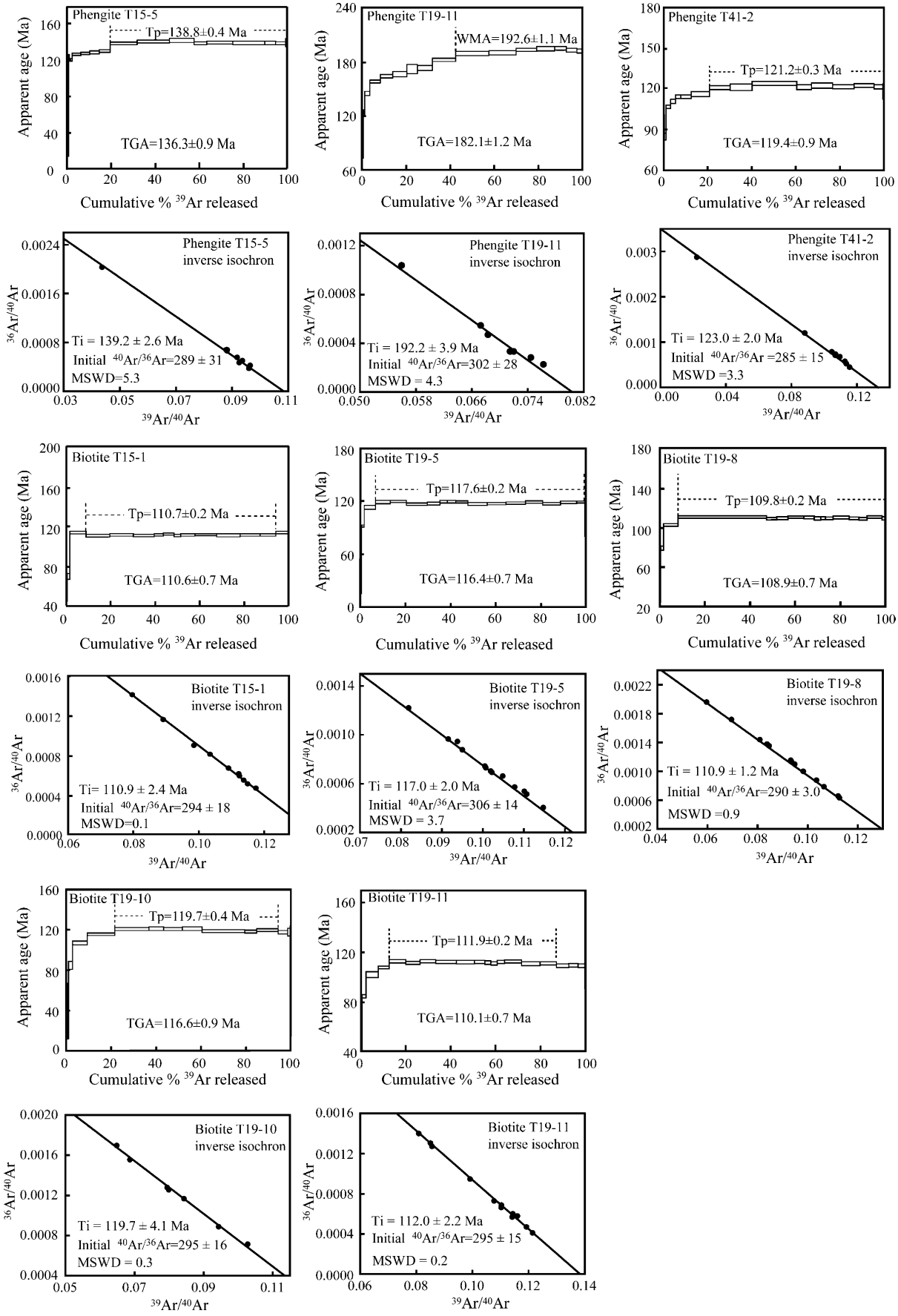

Fig. 6. Age spectra and inverse isochron plots for phengite and biotite samples from the Tan–Lu fault zone at the eastern edge of the Dabie orogenic belt. TGA: total gas age; T_p: plateau age; T_i: inverse isochron age; WMA: weighted mean age.

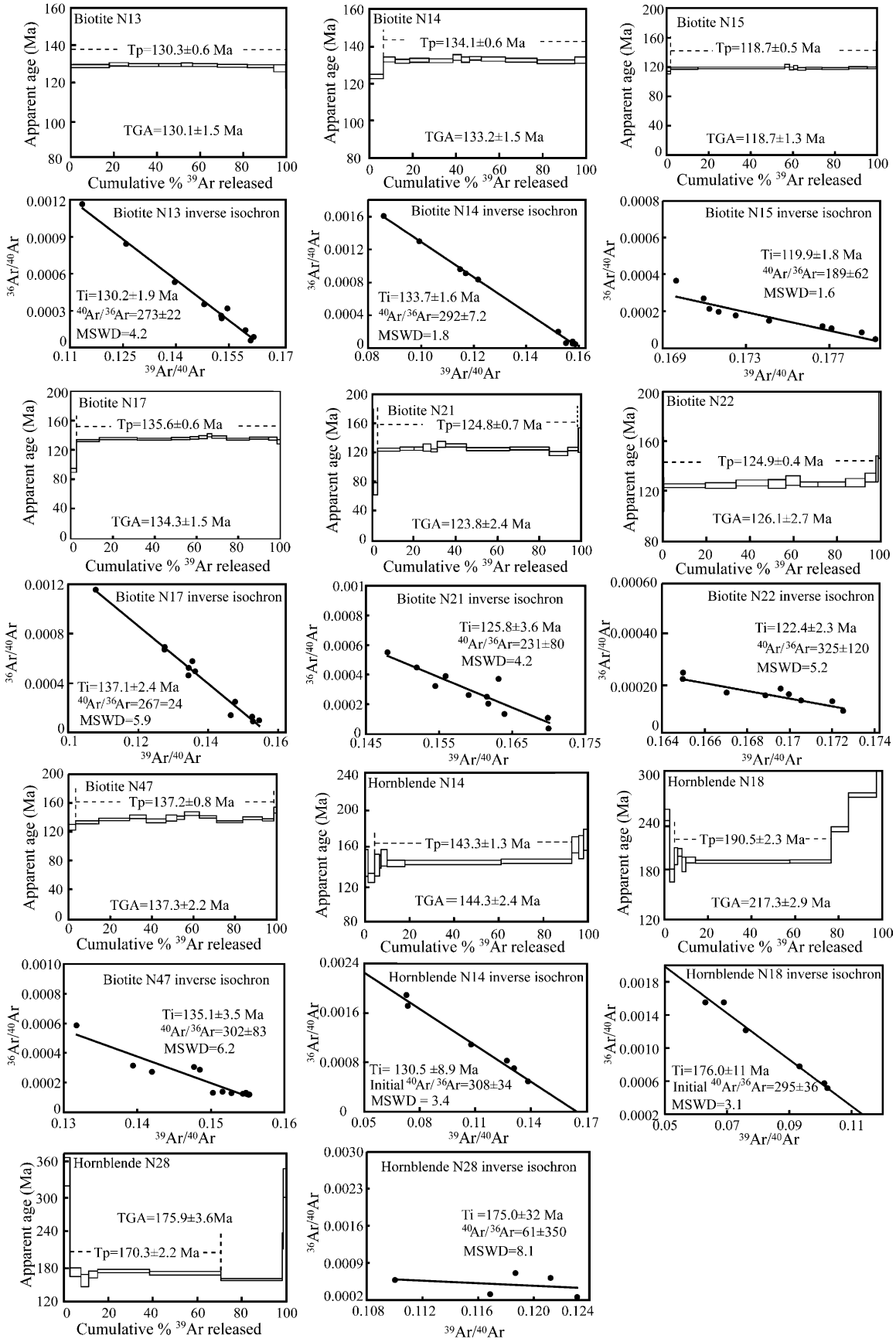

Fig. 7. Age spectra and inverse isochron plots for biotite and hornblende samples from the southern Zhangbaling part of the Tan–Lu fault zone. TGA: total gas age; T_p: plateau age; T_i: inverse isochron age.

considered that the lower temperature steps of the phengite sample with younger apparent ages are the result of partial resetting during the Tan–Lu faulting while its higher temperature steps mainly retain thermochronological information about the Dabie orogeny. In contrast, the biotite T19-11, separated from the same sample and with a lower closure temperature, gives an Early Cretaceous age of 119.7±0.4 Ma.

The phengite sample T41-2 from another locality gives a plateau age of 121.2±0.3 Ma. This age conforms approximately with its TGA (119.4±0.9 Ma) and T_i (123.0±2.0 Ma) and is used for later interpretation.

5.2. The southern Zhangbaling belt

Matrix biotite N14 and porphyroclastic hornblende N14 (from the same mylonite sample) and matrix biotite N13 were collected from one quarry. A plateau age of 143.3±1.3 Ma was obtained from the hornblende N14. It matches its TGA (144.3±2.4 Ma) within errors. Considering errors, its inverse isochron age (130.5±8.9 Ma) is only slightly younger than its T_p. The biotite N14 from the same mylonite sample yields a plateau age of 134.1±0.6 Ma, which is consistent with its TGA (133.2±1.5 Ma) and T_i (133.7±1.6 Ma). Biotite N13 from the same quarry shows a plateau age of 130.3±0.6 Ma with its TGA of 130.1±1.5 Ma and T_i of 130.2±1.9 Ma. These three plateau ages are treated as being geologically meaningful.

Biotite separate N17 gives a plateau age of 135.6±0.6 Ma, which is consistent with its TGA (134.3±1.5 Ma) and T_i (137.1±2.4 Ma). It is noted that this plateau age is similar to that obtained from biotite N14. Plateau ages of 124.8±0.7 and 124.9±0.4 Ma were obtained from biotite separates N21 and N22, respectively, from the same quarry (Fig. 2). They agree with their TGA and T_i. Biotite N47 yields a plateau age of 137.2±0.8 Ma, also consistent with its TGA (137.3±2.2 Ma) and T_i (135.1±3.5 Ma). These four plateau ages are also considered as being geologically meaningful.

Biotite N15 gives a plateau age of 118.7±0.5 Ma, which is consistent with its TGA (118.7±1.3 Ma) and T_i (119.9±1.8 Ma). However, it is noted that its initial $^{40}Ar/^{36}Ar$ value is 189±62, which is much younger than the atmospheric ratio of 295.5, probably indicating that the biotite experienced ^{39}Ar loss. Therefore, these ages are not used for geological interpretation in this paper.

Porphyroclastic hornblende N18 yields a plateau age of 190.5±2.3 Ma (Early Jurassic). Its age spectra show a U-shape (Fig. 7), indicating the presence of excess Ar, and as such its TGA (217.3±2.9 Ma) is older than the plateau age. Its inverse isochron age is 176.0±11 Ma, and is associated with an initial $^{40}Ar/^{36}Ar$ ratio of 309±26 and MSWD of 3.9. The southern Zhangbaling part of the Tan–Lu fault zone overprints on orogenic rocks that belonged to the Dabie–Sulu belt. Hacker et al. (2000) recorded that hornblende from metamorphic rocks in the Dabie belt commonly contains excess Ar. Chen et al. (1995) obtained a hornblende $^{40}Ar/^{39}Ar$ plateau age of 192.7±0.3 Ma from a gneiss in the Dabie UHP belt and interpreted it as a cooling age for the orogeny. It is inferred on this basis that the plateau age of 190.5±2.3 Ma for hornblende N18 roughly recorded a cooling age of retrograde metamorphism related to the Dabie–Sulu orogeny. This implies that Early Jurassic $^{40}Ar/^{39}Ar$ ages predominated in the high-grade rocks in the southern Zhangbaling belt before the Tan–Lu faulting. Porphyroclastic hornblende sample N28 gives a plateau age of 170.3±2.2 Ma. This agrees approximately with its TGA (175.9±3.6 Ma) and T_i (175.0±32 Ma). Its age spectra also show a U-shape and indicate the presence of excess Ar. Its unusual initial $^{40}Ar/^{39}Ar$ ratio (61±350) and high MSWD (8.1) suggest unreliability of the plateau age.

6. Interpretation and discussion

In dating mylonite porphyroclasts formed before mylonization, deformation temperatures play a critical role in interpretation. The deformation temperatures of the dated mylonites (Table 1) are all higher than the closure temperature of biotite (300±50 °C; Harrison et al., 1985). Therefore, the Ar system in the porphyroclastic biotite could have been totally reset and the obtained ages of both porphyroclastic and syn-mylonization biotite should represent cooling ages associated with the deformation event. The deformation temperatures of the dated prophyroclastic phengite and hornblende samples (Table 1) are higher than, or close to, the closure temperature range of white mica (350±50 °C; Dunlap, 1997) and hornblende (500±50 °C; Harrison, 1981; Reddy et al., 1997), and their ages could represent deformation ages, cooling ages or partial resetting ages (Lin, 2001). Phengite T19-11 (WMA, 192.6±1.1 Ma), hornblendes N18 (T_p=190.5±2.3 Ma) and N28 (T_p=170.3±2.2 Ma) from the Tan–Lu fault zone mainly record pre-mylonization metamorphic ages. Their Ar systems were not significantly reset during the Early Cretaceous faulting.

A plateau age of 138.8±0.4 Ma for phengite T15-5 is interpreted here as close to the cooling age of the Tan–Lu strike-slip faulting; it is the oldest cooling age obtained for the Tan–Lu faulting at the eastern edge of the Dabie belt. The deformation temperature estimate for the sample (400–450 °C) is close to the upper limit of the white mica closure temperature range. It is inferred that the plateau age of 138.8±0.4 Ma is close to the time of deformation associated with the Tan–Lu strike-slip motion. The plateau age of 110.7±0.2 Ma for biotite T15-1 from the same quarry is interpreted as the age at which the biotite cooled through its closure temperature after the Tan–Lu strike-slip faulting. The lower closure temperature of biotite and slow cooling made this cooling age quite a lot younger than that of the phengite (T15-5). The older phengite age and younger biotite age from the same quarry also demonstrate that the younger age of biotite with lower closure temperature

should represent a cooling age rather than a later ongoing deformation age. Based on the two cooling ages and the different closure temperatures for white mica (ca. 350 °C) and biotite (ca. 300 °C), a cooling rate of 1.78 °C Ma^{-1} is estimated from this part of the Tan–Lu ductile shear zone.

The plateau age of 121.2±0.3 Ma for phengite T41-2 from another locality is also interpreted as a cooling age. This age is younger than that of phengite T15-5, probably due to the sample being subjected to higher deformation temperature (500–550 °C), the highest temperature range experienced in this part of the Tan–Lu shear zone. During slow cooling after faulting, the white mica that experienced higher temperatures during deformation would pass through its closure temperature later than the white mica that experienced lower temperature during deformation. The difference between the two phengite ages also suggests a slow cooling rate after the Tan–Lu strike-slip faulting.

The four biotite plateau ages of 119.7±0.4 (T19-10), 117.6±0.2 (T19-5), 111.9±0.2 (T19-11) and 109.8±0.2 Ma (T19-8) obtained from the same quarry are considered here to represent cooling ages related to the Tan–Lu faulting. The samples were collected from each of the four small shear belts in this quarry. Apart from dating errors from the $^{40}Ar/^{39}Ar$ technique, different intensity of shear heating might be responsible for the differences of the cooling ages.

One hornblende and six biotite samples from the southern Zhangbaling belt all yield reliable Early Cretaceous plateau ages. The plateau age of 143.3±1.3 Ma for hornblende N14 is interpreted as a deformation age or cooling age very close to the Tan–Lu strike-slip motion because its deformation temperature (ca. 500 °C) is almost equal to the closure temperature of hornblende (500±50 °C). The plateau age of 134.1±0.6 Ma for syn-mylonization biotite N14 from the same mylonite sample represents a cooling age, as does the plateau age of 130.3±0.6 Ma for syn-mylonization biotite N13 from the same quarry. The difference of 4 Ma between the two biotite cooling ages might be due to dating errors or inhomogeneous shear heating. The hornblende and biotite plateau ages of the sample N14 and the different closure temperatures for biotite and hornblende can be used to calculate a cooling rate of 21.7 °C Ma^{-1} for this part of the shear belt, much higher than that obtained from the eastern edge of the Dabie belt (1.78 °C Ma^{-1}).

The plateau age of 135.6±0.6 Ma for biotite N17 from another locality is also interpreted as a cooling age. This age agrees with that of biotite N14 within errors. The biotite plateau age of 137.2±0.8 Ma (N47), the oldest biotite plateau age obtained in this study, is also considered as a cooling age. This age further constrains the sinistral motion to before 137 Ma. The plateau ages of 124.8±0.7 (biotite N21) and 124.9±0.4 Ma (biotite N22) from another locality are interpreted as cooling ages. These younger ages show the inhomogeneous cooling history in the southern Zhangbaling belt.

The hornblende, phengite and biotite $^{40}Ar/^{39}Ar$ ages are Early Cretaceous with some exceptions noted and explained above. The hornblende plateau age of 143.3 Ma, the oldest Early Cretaceous age obtained in this study, is interpreted as representing the time of sinistral strike-slip motion on the Zhangbaling part of the Tan–Lu fault zone. The oldest cooling age obtained from the eastern edge of the Dabie belt is 138.8 Ma (phengite T15-5), and should be close to the deformation age of the Tan–Lu strike-slip faulting. It is highly likely that the sinistral motion along the Tan–Lu fault zone at the eastern edge of the Dabie belt took place at the same time as in the southern Zhangbaling belt, i.e. in the earliest Early Cretaceous. Other $^{40}Ar/^{39}Ar$ phengite and biotite ages obtained from the southern part of the Tan–Lu fault zone represent different cooling ages when the minerals passed through their various closure temperatures. It is concluded on the basis of these $^{40}Ar/^{39}Ar$ ages that the large-scale strike-slip ductile shear belts in the southern part of the Tan–Lu fault zone were produced in the earliest Early Cretaceous, significantly after the NCB–SCB collision in the Triassic (Hacker et al., 2000).

Convergence and compression related to the NSB–SCB collision had ceased before the Early Cretaceous (Hacker et al., 2000; Ratschbacher et al., 2000; Faure et al., 2003). Therefore, the sinistral motion of the Tan–Lu fault zone in the Early Cretaceous cannot be attributed to the collision. Engebretson et al. (1985) and Maruyama et al. (1997) pointed out that the Izanagi plate of the Pacific plate subducted highly obliquely (towards the NNW) beneath the East Asian continent at a high speed in the Early Cretaceous. Xu et al. (1993), Xu and Zhu (1994) and Zhu and Xu (1997) proposed that the strike-slip movement of the Tan–Lu fault zone in East China in the Late Jurassic–Early Cretaceous was caused by this oblique subduction. A series of NE–NNE-trending, sinistral faults were associated with the Tan–Lu sinistral faulting during Late Jurassic to Early Cretaceous (Xu et al., 1993). According to this interpretation, the entire East China continent was subjected to intense transpression along the NNE-trending zone due to the Pacific oblique subduction. This sinistral faulting in East China was followed by, or associated with, voluminous intermediate magmatism in the Early Cretaceous (Zhou and Li, 2000). After the magmatism, regional extension, represented by the development of a series of Late Cretaceous to Paleogene extensional basins, occurred in East China including the Tan–Lu fault zone (Zhu et al., 2001b). This extension is believed to have resulted from lithospheric delamination (Zhou and Li, 2000) related to the low-speed, orthogonal subduction of the Pacific plate (Engebretson et al., 1985; Maruyama et al., 1997). It is inferred that the magmatism marked a transition from the Early Cretaceous sinistral faulting to the Late Cretaceous extension. The Tan–Lu strike-slip movement in the Early Cretaceous thus represents the onset of Pacific plate tectonism in East China (Zhu et al., 2004).

The $^{40}Ar/^{39}Ar$ ages obtained in this study demonstrate

that the large-scale, sinistral, ductile shear belts in the southern part of the Tan–Lu fault zone were developed in the earliest Early Cretaceous. No fault structures older than Early Cretaceous have been identified in the southern part of the Tan–Lu fault zone in this study. The $^{40}Ar/^{39}Ar$ ages also offer no evidence of syn-orogenic faulting in the Tan–Lu fault zone. However, it cannot be ruled out that evidence for syn-orogenic faulting was obliterated by the later shearing or is covered by later basins beside the present Tan–Lu exposures. More detailed work is thus needed to test the possibility of syn-orogenic Tan–Lu faulting. In spite of this uncertainty, our results indicate that the Early Cretaceous Tan–Lu faulting event is at least partly responsible for the 550 km, sinistral offset of the Dabie and Sulu orogenic belts.

7. Conclusions

Strike-slip structures of the southern part of the Tan–Lu fault zone are represented by the NE-trending, sinistral ductile shear belts developed under medium to upper greenschist facies conditions. Biotite, phengite and hornblende separates from mylonites in the shear belts were analysed using the $^{40}Ar/^{39}Ar$ technique. Prophyroclastic phengite T19-11 (WMA, 192.6 Ma) from the eastern edge of the Dabie belt and hornblendes N18 ($T_p = 190.5$ Ma) and N28 ($T_p = 170.3$ Ma) from the southern Zhangbaling belt record pre-mylonization, metamorphic ages related to the NSB–SCB collision. The other samples all yield Early Cretaceous $^{40}Ar/^{39}Ar$ ages. The hornblende plateau age of 143.3 Ma (N14) is interpreted as representing the time of sinistral strike-slip motion on the Zhangbaling part of the Tan–Lu fault zone. The plateau age of 138.8 Ma for phengite T15-5 is considered as being close to the deformation time of the Tan–Lu strike-slip faulting. It is highly likely that the sinistral strike-slip motion along the Tan–Lu fault zone at the eastern edge of the Dabie belt took place at the same time, in the earliest Early Cretaceous, as in the southern Zhangbaling belt. Other $^{40}Ar/^{39}Ar$ phengite and biotite ages represent cooling ages when the minerals passed through their various closure temperatures. It is concluded on the basis of these $^{40}Ar/^{39}Ar$ ages that the sinistral ductile shear belts in the southern part of the Tan–Lu fault zone were developed in the earliest Early Cretaceous.

This intense sinistral movement of the Tan–Lu fault zone is considered to be related to the highly oblique subduction of the Izanagi plate. This conclusion implies that strike-slip motion on the Tan–Lu fault zone at least partly contributed to the 550 km offset of the Dabie and Sulu orogenic belts in the Early Cretaceous.

Acknowledgements

This study was funded by the National Natural Science Foundation of China (grant number 40272094). We gratefully acknowledge the support and advice on the $^{40}Ar/^{39}Ar$ analyses from Mr Chen Wen from the Ar–Ar Laboratory, Institute of Geology, Chinese Academy of Geological Sciences and Mr Sang Haiqing from the Ar–Ar Laboratory, Institute of Geology and Geophysics, Chinese Academy of Sciences. Many thanks to YD Zheng and Pat Meere for their constructive reviews, as well as Bill Fitches, Shoufa Lin and Jen Parks for their help with improving the manuscript.

Appendix. Detailed $^{40}Ar/^{39}Ar$ analytical results

T (°C)	$^{40}Ar/^{39}Ar$	$^{36}Ar/^{39}Ar$	$^{37}Ar/^{39}Ar$	$^{38}Ar/^{39}Ar$	$^{40}Ar^*/^{39}Ar_k$	^{39}Ar (%)	Age $\pm 1\sigma$ (Ma)
T15-1 biotite, $W = 0.040$ g, $J = 0.008628$, TGA $= 110.6 \pm 0.7$ Ma, $T_p = 110.7 \pm 0.2$ Ma (6–16 steps, 85% released ^{39}Ar)							
400	206.8570	0.6854	4.6752	0.3011	4.6761	0.06	71.0 ± 5.8
500	66.6233	0.1837	4.7589	0.1315	12.7137	0.20	187.8 ± 2.0
600	131.4166	0.4335	2.8001	0.2161	3.5287	0.24	54.0 ± 5.8
700	20.7644	0.0554	1.7291	0.0326	4.5210	0.96	69.0 ± 1.6
800	10.1493	0.0089	0.0574	0.0218	7.5219	7.35	113.4 ± 0.8
850	8.9278	0.0055	0.0725	0.0142	7.2942	10.75	110.1 ± 0.6
880	8.9076	0.0053	0.0626	0.0142	7.3338	10.56	110.7 ± 0.7
910	8.9268	0.0055	0.0545	0.0142	7.2953	9.44	110.1 ± 0.6
940	11.2055	0.0131	0.0857	0.0160	7.3354	4.10	110.7 ± 0.7
1000	10.1478	0.0092	0.0636	0.0148	7.4214	4.90	112.0 ± 0.6
1050	12.5244	0.0177	0.1114	0.0170	7.2898	2.84	110.0 ± 0.7
1130	9.6650	0.0079	0.0657	0.0146	7.3377	6.34	110.7 ± 0.6
1180	8.7149	0.0045	0.0477	0.0137	7.3772	9.89	111.3 ± 0.7
1230	8.5224	0.0041	0.0477	0.0138	7.3135	10.63	110.4 ± 0.7
1260	8.8121	0.0049	0.0457	0.0140	7.3691	8.78	111.2 ± 0.7
1300	9.1819	0.0062	0.0395	0.0144	7.3448	7.14	110.8 ± 0.7
1350	9.6209	0.0071	0.0427	0.0158	7.5101	5.61	113.3 ± 0.7
1400	61.7367	0.1871	2.5992	0.0163	6.6392	0.21	100.0 ± 6.8

T (°C)	$^{40}Ar/^{39}Ar$	$^{36}Ar/^{39}Ar$	$^{37}Ar/^{39}Ar$	$^{38}Ar/^{39}Ar$	$^{40}Ar^*/^{39}Ar_k$	^{39}Ar (%)	Age$\pm1\sigma$ (Ma)
T15-5 phengite, $W=0.041$ g, $J=0.008697$, TGA$=136.3\pm0.9$ Ma, $T_p=138.8\pm0.4$ Ma (10–18 steps, 81% released ^{39}Ar)							
500	115.4202	0.3900	15.1862	0.2113	1.2500	0.10	19.5±4.8
600	61.3036	0.1954	12.7323	0.1325	4.5113	0.18	69.0±12
680	64.7599	0.2150	6.6752	0.0953	1.7007	0.19	26.0±6.3
780	24.4037	0.0553	0.3084	0.0306	8.0760	0.64	122.5±1.7
830	14.7306	0.0232	0.3365	0.0178	7.9097	1.29	120.0±0.7
910	10.9783	0.0090	0.1468	0.0153	8.3236	3.77	126.0±0.7
940	10.6620	0.0077	0.1068	0.0148	8.3826	4.04	126.9±0.7
970	10.6004	0.0072	0.1101	0.0147	8.4641	4.47	128.1±0.9
1000	10.3492	0.0062	0.5548	0.0194	8.5636	4.78	129.6±0.7
1030	10.4094	0.0043	0.2114	0.0176	9.1404	12.28	138.0±0.7
1060	10.4404	0.0039	0.2535	0.0163	9.2947	14.79	140.2±0.7
1080	10.8314	0.0050	0.3747	0.0178	9.3647	11.16	141.2±1.2
1110	10.8975	0.0060	0.6177	0.0204	9.1536	5.78	138.2±0.7
1140	10.7432	0.0053	0.2425	0.0171	9.1945	11.69	138.8±0.7
1170	10.7072	0.0053	0.1555	0.0160	9.1589	14.68	138.3±0.9
1200	11.3613	0.0074	0.0357	0.0146	9.1798	4.85	138.6±1.1
1250	11.4207	0.0076	0.0755	0.0151	9.1624	4.62	138.3±0.8
1300	22.8519	0.0464	0.6376	0.0272	9.1850	0.69	138.6±2.3
T19-5 biotite, $W=0.038$ g, $J=0.008678$, TGA$=116.4\pm0.7$ Ma, $T_p=117.6\pm0.2$ Ma (5–17 steps, 89% released ^{39}Ar)							
500	109.6196	0.3514	3.8426	0.1386	6.0744	0.15	92.7±4.4
600	50.0061	0.1651	5.9495	0.0737	1.6372	0.26	25.0±5.3
700	15.3609	0.0319	0.6995	0.0229	5.9867	1.40	91.4±0.6
780	10.0794	0.0090	0.1587	0.0154	7.4131	5.03	112.5±1.3
830	9.8412	0.0069	0.0456	0.0183	7.8115	6.46	118.3±0.9
880	9.8200	0.0067	0.0500	0.0144	7.8465	7.16	118.8±0.6
930	9.0956	0.0049	0.2851	0.0179	7.6624	9.20	116.1±0.7
960	10.6975	0.0102	0.6586	0.0398	7.7184	5.77	117.0±0.6
990	12.2597	0.0150	0.1172	0.0163	7.8457	3.26	118.8±0.7
1040	10.9638	0.0106	0.1469	0.0159	7.8488	3.71	118.9±0.7
1090	9.9571	0.0072	0.0872	0.0147	7.8266	5.28	118.5±0.6
1140	9.0514	0.0046	0.0565	0.0140	7.6833	8.70	116.4±0.7
1170	8.7303	0.0035	0.2626	0.0164	7.6970	8.30	116.6±0.6
1200	9.3058	0.0053	0.0553	0.0143	7.7388	8.48	117.3±0.7
1230	9.8124	0.0067	0.0500	0.0159	7.8173	7.82	118.4±0.7
1260	9.5571	0.0063	0.0576	0.0146	7.6964	7.77	116.6±0.7
1290	9.9904	0.0074	0.0722	0.0147	7.7982	7.14	118.1±0.8
1320	10.5511	0.0093	0.0977	0.0149	7.8191	3.60	118.4±0.7
1370	26.6999	0.0725	1.2789	0.0332	5.3683	0.51	82.1±1.4
T19-8 biotite, $W=0.039$ g, $J=0.008729$, TGA$=108.9\pm0.7$ Ma, $T_p=109.8\pm0.2$ Ma (6–18 steps, 92% released ^{39}Ar)							
400	308.4636	1.0320	3.6883	0.3653	3.7882	0.04	59.0±23
500	130.6573	0.4318	4.8483	0.1394	3.4184	0.09	53.0±10
600	51.0453	0.1675	5.3548	0.0656	1.9436	0.29	30.3±2.5
700	16.8568	0.0398	0.7168	0.0241	5.1511	1.27	79.3±1.0
800	9.6085	0.0099	0.1120	0.0152	6.6970	6.40	102.5±0.6
850	8.9513	0.0058	0.0912	0.0162	7.2310	39.30	110.4±0.6
880	10.7427	0.0122	0.0712	0.0152	7.1446	4.48	109.1±0.7
910	10.5874	0.0116	0.0696	0.0152	7.1740	4.99	109.6±0.7
940	9.4114	0.0073	0.0480	0.0143	7.2495	7.02	110.7±0.6
970	10.2093	0.0101	0.0690	0.0151	7.2192	4.68	110.2±0.6
1020	11.9829	0.0164	0.0784	0.0165	7.1473	2.81	109.2±0.7
1070	14.4589	0.0247	0.1306	0.0181	7.1634	2.11	109.4±0.7
1120	12.4195	0.0178	0.0807	0.0165	7.1579	3.37	109.3±0.6
1170	9.6958	0.0084	0.0484	0.0144	7.1986	7.02	109.9±0.7
1200	10.7381	0.0121	0.0554	0.0154	7.1675	4.47	109.5±0.7
1250	11.8650	0.0160	0.0772	0.0163	7.1494	3.56	109.2±0.6
1300	8.8985	0.0056	0.0519	0.0189	7.2512	6.73	110.7±0.6
1350	16.9128	0.0330	0.2249	0.0202	7.1717	1.27	109.5±0.8
1400	113.3941	0.3688	1.6070	0.1210	4.5359	0.10	70.0±6.8
T19-10 biotite, $W=0.040$ g, $J=0.008819$, TGA$=116.6\pm0.9$ Ma, $T_p=119.7\pm0.4$ Ma (7–13 steps, 73% released ^{39}Ar)							
400	148.3528	0.4915	3.5003	0.1893	3.3529	0.27	53.0±5.8
500	255.6970	0.8593	20.4000	0.2528	3.2827	0.16	51.0±8.4
600	70.4592	0.2353	6.8121	0.0833	1.4045	0.56	22.0±5.3

(*continued on next page*)

T (°C)	$^{40}Ar/^{39}Ar$	$^{36}Ar/^{39}Ar$	$^{37}Ar/^{39}Ar$	$^{38}Ar/^{39}Ar$	$^{40}Ar^*/^{39}Ar_k$	^{39}Ar (%)	Age $\pm 1\sigma$ (Ma)
700	25.6632	0.0687	1.3077	0.0317	5.4523	1.89	84.7±2.1
800	13.1899	0.0213	0.2273	0.0180	6.9104	6.60	106.7±1.1
880	10.7600	0.0111	0.1411	0.0155	7.4751	12.10	115.2±0.7
960	10.6051	0.0094	0.0596	0.0147	7.8201	15.17	120.3±0.7
1010	14.5075	0.0227	0.1734	0.0180	7.8230	6.60	120.4±0.8
1090	12.5294	0.0160	0.1712	0.0158	7.8232	8.35	120.4±0.8
1140	12.4806	0.0157	0.1343	0.0167	7.8321	8.77	120.5±0.8
1190	9.7472	0.0069	0.0340	0.0142	7.6935	19.10	118.4±0.8
1220	15.3561	0.0261	0.1898	0.0186	7.6647	5.39	118.0±0.8
1270	11.8392	0.0138	0.1453	0.0160	7.7647	9.47	119.5±0.7
1300	16.7161	0.0308	0.2354	0.0192	7.6388	4.42	117.6±0.8
1350	50.7492	0.1461	0.9558	0.0482	7.6541	0.91	117.8±3.1
1400	166.0424	0.5377	3.7304	0.1451	7.4449	0.24	115.0±6.3
T19-11 biotite, W=0.039 g, J=0.00887, TGA=110.1±0.7 Ma, T_p=111.9±0.2 Ma (7-18 steps, 74% released ^{39}Ar)							
400	490.6629	1.6504	9.9950	0.5280	3.7032	0.02	58.0±21
500	181.3236	0.5905	3.0464	0.1820	7.0565	0.09	110.0±7.9
600	40.3698	0.1281	5.5934	0.0537	2.9105	0.36	46.0±2.5
700	13.1441	0.0263	0.7751	0.0208	5.4233	1.88	84.8±0.7
780	9.2065	0.0090	0.1807	0.0153	6.5599	5.29	102.0±1.2
810	9.4313	0.0084	0.0942	0.0149	6.9624	5.07	108.1±0.6
840	9.0064	0.0059	0.0389	0.0152	7.2670	7.31	112.7±0.6
870	8.9956	0.0061	0.0733	0.0142	7.1865	6.40	111.5±0.6
900	8.7103	0.0049	0.2746	0.0183	7.2673	6.98	112.7±0.7
930	8.3709	0.0039	0.0428	0.0135	7.2293	9.26	112.1±0.6
960	8.1948	0.0033	0.1398	0.0157	7.2163	7.96	111.9±0.8
990	10.0062	0.0094	0.0731	0.0148	7.2280	4.59	112.1±0.6
1020	12.2372	0.0171	0.1396	0.0168	7.2024	2.68	111.7±0.8
1070	11.6421	0.0151	0.1042	0.0163	7.1670	2.95	111.2±0.6
1120	11.5780	0.0147	0.0703	0.0158	7.2425	3.18	112.3±0.6
1170	9.2220	0.0066	0.0610	0.0144	7.2573	7.66	112.5±0.7
1200	8.5973	0.0049	0.0573	0.0138	7.1392	8.14	110.8±0.7
1230	8.6883	0.0051	0.0713	0.0139	7.1682	7.18	111.2±0.6
1260	9.1056	0.0070	0.1030	0.0143	7.0359	5.58	109.2±0.8
1300	10.0589	0.0101	0.1291	0.0152	7.0672	4.23	109.7±0.7
1350	11.3274	0.0146	0.1983	0.0160	7.0364	3.03	109.2±0.7
1400	62.6120	0.1917	3.2656	0.0632	6.2061	0.16	96.7±2.9
T19-11 phengite, W=0.039 g, J=0.009030, TGA=182.1±1.2 Ma, WMA=192.6±1.1 Ma (12–18 steps, 57% released ^{39}Ar)							
400	225.9198	0.7512	7.8585	0.2075	4.5346	0.06	72.0±29
500	92.4900	0.3080	3.1025	0.0819	1.6884	0.13	27.0±16
600	50.2088	0.1533	1.8179	0.0521	5.0482	0.30	80.4±3.5
700	29.6802	0.0739	0.5559	0.0312	7.8876	0.62	124.1±1.8
800	14.7907	0.0185	0.0737	0.0172	9.3261	2.38	145.9±1.0
880	12.9053	0.0092	0.0386	0.0151	10.1751	4.78	158.6±0.9
930	12.9037	0.0078	0.0475	0.0147	10.5998	5.65	164.9±0.9
960	13.2524	0.0086	0.3452	0.0227	10.7246	6.48	166.8±1.3
990	13.5188	0.0081	0.4793	0.2222	11.1445	4.65	173.0±2.6
1020	13.2618	0.0072	0.7181	0.0175	11.1934	6.93	173.7±1.5
1050	13.1004	0.0045	0.1877	0.0165	11.7892	10.48	182.5±0.9
1080	13.1506	0.0029	0.0400	0.0162	12.3041	15.16	190.1±1.1
1110	13.4695	0.0038	0.1656	0.0155	12.3673	12.51	191.0±1.1
1140	13.9300	0.0046	0.2817	0.0159	12.5888	9.20	194.2±1.1
1170	14.0240	0.0047	0.2961	0.0191	12.6574	8.23	195.2±1.3
1200	14.6744	0.0069	0.4230	0.0205	12.6789	5.26	195.5±1.2
1230	14.9172	0.0080	0.1581	0.0154	12.5614	4.83	193.8±1.1
1280	17.9187	0.0185	0.3763	0.0185	12.4681	2.15	192.5±1.2
1330	61.0748	0.1910	2.2390	0.0613	4.8093	0.20	76.7±3.4
T41-2 phengite, W=0.039 g, J=0.009336, TGA=119.4±0.9 Ma, T_p=121.2±0.3 Ma (9–17 steps, 79% released ^{39}Ar)							
500	121.6412	0.3955	10.7443	0.1332	5.5838	0.16	92.0±7.4
600	55.5756	0.1711	7.1296	0.0710	5.5568	0.26	91.2±5.1
700	26.5870	0.0729	1.1889	0.0304	5.1199	0.62	84.2±1.4
800	13.9412	0.0253	0.2750	0.0190	6.4724	2.11	105.8±0.7
850	13.0819	0.0215	0.1802	0.0179	6.7429	2.24	110.1±0.8
900	12.3682	0.0184	0.1827	0.0169	6.9548	2.39	113.5±0.6
950	10.1622	0.0108	0.0834	0.0149	6.9719	4.84	113.8±0.7

T (°C)	$^{40}Ar/^{39}Ar$	$^{36}Ar/^{39}Ar$	$^{37}Ar/^{39}Ar$	$^{38}Ar/^{39}Ar$	$^{40}Ar^*/^{39}Ar_k$	^{39}Ar (%)	Age$\pm1\sigma$ (Ma)
1000	9.0064	0.0065	0.3484	0.0172	7.0955	8.38	115.7±1.0
1030	9.1687	0.0061	0.0328	0.0141	7.3729	9.23	120.1±0.7
1060	8.8930	0.0051	0.3745	0.0166	7.4009	10.00	120.5±1.3
1090	8.6812	0.0038	0.0769	0.0176	7.5636	20.30	123.1±0.7
1120	9.5851	0.0075	0.2821	0.0178	7.3960	6.69	120.5±0.9
1150	8.8327	0.0047	0.2269	0.0152	7.4692	9.63	121.6±0.8
1180	9.3973	0.0068	0.0383	0.0141	7.3991	9.63	120.5±0.8
1230	9.4019	0.0065	0.0365	0.0141	7.4689	9.19	121.6±0.6
1280	11.3992	0.0135	0.0651	0.0157	7.3987	4.00	120.5±0.8
1335	46.1019	0.1322	0.8134	0.0484	7.1077	0.33	116.0±5.3
N13 biotite, W=0.1206 g, J=0.012345, TGA=130.1±1.5 Ma, T_p=130.3±0.6 Ma (1–10 steps, 100% released ^{39}Ar)							
800	7.9471	0.0067	0.4680	0.0216	6.0121	17.74	129.16±1.32
850	7.1527	0.0038	1.4995	0.0211	6.1326	8.96	131.65±1.47
900	6.5426	0.0017	0.5758	0.0205	6.0914	13.91	130.80±1.28
950	6.5408	0.0016	0.3882	0.0206	6.0924	10.47	130.82±1.35
1000	6.7506	0.0023	0.7638	0.0207	6.1149	5.24	131.29±1.59
1100	6.2055	0.0003	0.0005	0.0210	6.0993	11.55	130.96±1.29
1150	6.1774	0.0005	0.4016	0.0207	6.0501	13.91	129.94±1.30
1200	6.2644	0.0009	0.3781	0.0203	6.0347	12.25	129.62±1.28
1300	6.4785	0.0021	0.7262	0.0203	5.9236	5.55	127.32±3.11
1400	8.8022	0.0103	0.0005	0.0203	5.7686	0.42	124.10±5.78
N14 biotite, W=0.1089 g, J=0.012345, TGA=133.2±1.5 Ma, T_p=134.1±0.6 Ma (2–12 steps, 94% released ^{39}Ar)							
800	14.608	0.0306	1.3993	0.0369	5.6713	6.40	122.08±1.48
830	11.646	0.0187	2.0437	0.0348	6.2701	5.33	134.50±1.78
860	10.085	0.0132	0.3561	0.0334	6.2082	6.71	133.22±1.45
900	8.5534	0.0079	0.3207	0.0325	6.2397	8.98	133.87±1.45
950	8.2162	0.0069	0.8052	0.0323	6.2242	11.04	133.55±1.41
1000	8.7143	0.0084	1.3734	0.0325	6.3421	3.88	135.98±2.02
1050	8.5452	0.0079	0.5661	0.0331	6.2625	3.75	134.34±1.98
1150	6.4440	0.0004	0.1246	0.0325	6.3248	5.45	135.63±1.57
1200	6.3362	0.0004	0.8986	0.0331	6.2827	11.15	134.76±1.49
1250	6.3145	0.0003	0.2964	0.0332	6.2405	14.57	133.89±1.35
1300	6.3320	0.0005	0.0005	0.0313	6.1885	17.32	132.81±1.30
1400	6.5711	0.0014	1.1073	0.0311	6.2476	5.42	134.03±2.31
N14 hornblende, W=0.1735 g, J=0.012345, TGA=144.3±2.4 Ma, T_p=143.9±1.3 Ma (3–10 Steps, 93% released ^{39}Ar)							
800	49.652	0.1492	14.404	0.0711	6.6600	1.61	142.54±9.98
900	19.573	0.0476	4.8081	0.0482	5.8780	2.88	126.37±3.79
1000	13.692	0.0258	6.2320	0.0675	6.5430	2.22	140.13±8.37
1050	13.567	0.0232	21.933	0.0928	9.0898	0.62	143.70±4.70
1100	9.2795	0.0100	8.1026	0.1637	6.9631	2.74	148.21±5.90
1150	7.8815	0.0064	8.6496	0.2213	6.6332	7.98	141.99±2.20
1200	7.6539	0.0053	7.7197	0.2361	6.6766	42.98	142.88±1.42
1240	7.2419	0.0035	7.1260	0.2282	6.7458	31.84	144.30±1.50
1280	12.5245	0.0200	13.105	0.2225	7.6153	2.96	162.09±5.28
1340	9.9676	0.0102	7.1459	0.2386	7.4999	1.95	159.74±7.72
1400	9.5461	0.0090	13.109	0.2364	7.8846	2.22	167.56±6.80
N15 biotite, W=0.1076 g, J=0.012353, TGA=118.7±1.3 Ma, T_p=118.7±0.5 Ma (2–11steps, 98% released ^{39}Ar)							
700	6.2263	0.0038	1.2629	0.0180	5.2093	1.72	112.51±1.73
800	5.8235	0.0011	0.0005	0.0160	5.4919	13.03	118.41±1.18
900	5.5790	0.0002	0.1056	0.0156	5.5139	41.24	118.87±1.16
950	5.7431	0.0008	2.1121	0.0162	5.6612	2.19	121.94±2.03
1000	5.8394	0.0012	0.0005	0.0159	5.4823	1.96	118.21±1.76
1050	5.8946	0.0021	3.7231	0.0165	5.5519	1.99	119.66±2.55
1100	5.8484	0.0015	0.7733	0.0167	5.4510	3.82	117.56±1.71
1150	5.6596	0.0006	0.4206	0.0163	5.4993	7.74	118.57±1.26
1200	5.5998	0.0004	0.0005	0.0158	5.4671	12.63	117.89±1.15
1250	5.6454	0.0006	0.7202	0.0157	5.5303	8.93	119.21±1.22
1300	5.7957	0.0010	0.2762	0.0158	5.5214	4.22	119.03±1.32
1400	7.8050	0.0072	9.3299	0.0240	6.3954	0.53	137.17±6.89
N17 biotite, W=0.1063 g, J=0.012345, TGA=134.3±1.5 Ma, T_p=135.6±0.6 Ma (2–13 steps, 97% released ^{39}Ar)							
700	23.366	0.0662	6.0644	0.0286	4.2456	2.75	92.16±2.65
800	9.2553	0.0107	1.1253	0.0154	6.1797	10.88	132.63±1.39
850	7.8402	0.0053	0.4675	0.0140	6.3144	17.86	135.41±1.36

(*continued on next page*)

T (°C)	$^{40}Ar/^{39}Ar$	$^{36}Ar/^{39}Ar$	$^{37}Ar/^{39}Ar$	$^{38}Ar/^{39}Ar$	$^{40}Ar^{*}/^{39}Ar_{k}$	^{39}Ar (%)	Age $\pm 1\sigma$ (Ma)
900	7.3339	0.0036	0.5160	0.0136	6.2971	16.42	135.06±1.34
950	7.4338	0.0039	0.5987	0.0137	6.3271	8.95	135.67±1.46
1000	7.8394	0.0054	1.7985	0.0140	6.3683	4.17	136.52±1.65
1050	7.4423	0.0034	0.0005	0.0137	6.4214	4.05	137.62±1.86
1100	6.8259	0.0010	0.0005	0.0132	6.5399	2.28	140.07±2.04
1150	6.5449	0.0006	0.5689	0.0132	6.4203	7.04	137.60±1.66
1200	6.4710	0.0006	0.0336	0.0131	6.2893	10.92	134.89±1.32
1250	6.5540	0.0008	0.7803	0.0131	6.3641	9.12	136.44±1.39
1300	6.7675	0.0017	0.8204	0.0135	6.3256	4.11	135.64±1.93
1400	7.3850	0.0043	0.0005	0.0142	6.1196	1.45	131.38±2.98
N18 hornblende, W=0.1076 g, J=0.012353, TGA=217.3±2.9 Ma, T_p=190.0±2.2 Ma (3–9 steps, 74% released ^{39}Ar)							
700	53.385	0.1231	9.9394	0.0489	110.91	0.49	350.10±12.50
800	13.159	0.0074	10.579	0.0599	43.841	1.80	245.90±6.10
900	11.398	0.0139	11.382	0.0525	8.1577	2.11	173.20±7.72
1000	14.489	0.0224	18.341	0.0804	9.3049	1.49	196.28±10.34
1050	15.827	0.0245	12.184	0.1526	9.5388	2.03	200.95±4.72
1100	13.139	0.0159	4.6960	0.1914	8.7999	1.77	186.16±8.96
1150	10.733	0.0083	10.087	0.2025	9.0704	4.45	191.59±3.54
1200	9.8947	0.0056	9.1578	0.1877	8.9617	43.27	189.41±1.85
1240	9.7922	0.0050	8.7577	0.1854	8.9842	18.95	189.86±1.95
1280	12.327	0.0079	12.386	0.1914	10.976	7.96	229.38±3.03
1340	14.418	0.0067	8.7812	0.1938	13.137	12.84	271.29±2.71
1400	36.164	0.0127	9.4046	0.2214	33.340	2.84	622.20±7.43
N21 biotite, W=0.1054 g, J=0.012353, TGA=123.8±2.4 Ma, T_p=124.8±0.7 Ma (2–13 steps, 98% released ^{39}Ar)							
700	6.7757	0.0171	20.334	0.0242	3.1996	2.54	69.93±8.26
800	6.7597	0.0037	1.4182	0.0232	5.7608	10.93	124.02±1.98
840	6.1905	0.0015	1.2427	0.0232	5.8234	6.46	125.32±1.85
870	6.1821	0.0013	0.0015	0.0234	5.8066	4.49	124.97±1.57
900	6.4166	0.0025	3.1361	0.0239	5.9006	3.83	126.92±5.01
950	6.5805	0.0030	0.1596	0.0247	5.7116	2.82	122.99±2.02
1050	6.4719	0.0021	3.1050	0.0236	6.0895	4.21	130.84±4.15
1100	6.0980	0.0008	2.2985	0.0229	6.0306	9.87	129.62±2.23
1150	5.8796	0.0002	0.6512	0.0230	5.7864	20.83	124.55±1.59
1200	5.8860	0.0006	1.6262	0.0235	5.8184	18.76	125.21±1.34
1250	6.1230	0.0024	1.2641	0.0232	5.4966	8.93	118.51±2.78
1300	6.2857	0.0017	0.0015	0.0249	5.7934	4.89	124.69±1.92
1400	7.1550	0.0057	12.289	0.0270	6.3870	1.44	137.00±16.89
N22 biotite, W=0.1105 g, J=0.012374, TGA=126.1±2.7 Ma, T_p=125.2±0.9 Ma (1–12 steps, 100% released ^{39}Ar)							
700	8.8682	0.0120	1.0050	0.0259	5.4027	0.30	116.74±13.96
800	6.0612	0.0012	0.7835	0.0237	5.7490	19.23	123.97±1.33
840	5.8641	0.0006	0.8530	0.0233	5.7514	14.12	124.02±2.00
870	5.7955	0.0003	2.0857	0.0232	5.8492	14.76	126.06±2.29
900	5.8121	0.0006	2.3448	0.0231	5.8219	8.11	125.49±3.25
1000	5.8966	0.0009	4.1828	0.0241	5.9575	6.58	128.31±3.72
1100	5.9866	0.0008	0.6707	0.0244	5.8045	7.96	125.13±1.69
1150	5.8829	0.0007	2.0158	0.0242	5.8173	12.79	125.40±2.00
1200	5.9216	0.0007	2.2266	0.0235	5.8785	8.95	126.67±3.36
1250	6.0603	0.0011	4.4536	0.0235	6.0687	4.93	130.62±3.65
1300	6.3854	0.0019	7.1871	0.0238	6.3694	1.49	136.86±11.72
1400	7.2474	0.0028	25.584	0.0248	8.4126	0.78	178.65±31.90
N28 hornblende, W=0.1746 g, J=0.012374, TGA=175.9±3.6 Ma, T_p=170.3±2.2 Ma (3–7 steps, 68% released ^{39}Ar)							
700	44.831	0.0848	77.487	0.1101	71.897	0.60	399.30±29.20
800	14.153	0.0058	55.384	0.0376	17.128	2.17	346.76±20.11
900	9.0842	0.0052	6.5609	0.0304	8.0463	4.95	171.23±6.86
1000	8.4247	0.0060	8.8297	0.0418	7.3311	3.45	156.65±10.71
1050	8.2466	0.0052	14.487	0.0113	7.8351	3.98	166.93±5.69
1100	8.5538	0.0027	4.6523	0.1390	8.1150	23.34	172.62±1.92
1150	8.1229	0.0018	4.6180	0.1372	7.9343	32.08	168.95±1.85
1200	7.5044	0.0015	5.0296	0.1298	7.4336	27.68	158.74±1.84
1240	9.8589	0.0005	13.141	0.0947	10.760	0.27	225.48±13.05
1300	17.020	0.0142	37.226	0.1035	15.940	1.14	324.75±24.42
1400	50.500	0.0380	57.858	0.1371	45.505	0.34	805.76±68.74
N47 biotite, W=0.1221 g, J=0.012415, TGA=137.3±2.2 Ma, T_p=137.2±0.8 Ma (2–12 steps, 95% released ^{39}Ar)							
700	6.2751	0.0055	15.898	0.0250	5.8411	3.35	126.29±3.93

T (°C)	$^{40}Ar/^{39}Ar$	$^{36}Ar/^{39}Ar$	$^{37}Ar/^{39}Ar$	$^{38}Ar/^{39}Ar$	$^{40}Ar^*/^{39}Ar_k$	^{39}Ar (%)	Age $\pm 1\sigma$ (Ma)
800	6.7346	0.0019	0.1762	0.0204	6.1695	11.14	133.14 ± 2.08
840	6.5442	0.0008	0.9089	0.0197	6.3606	14.68	137.11 ± 1.73
870	6.4767	0.0008	3.9523	0.0196	6.5340	8.14	140.71 ± 2.47
900	6.7729	0.0021	1.4580	0.0194	6.2641	9.39	135.11 ± 2.67
950	7.5891	0.0045	2.4650	0.0213	6.4511	5.31	138.99 ± 4.16
1000	7.0400	0.0019	0.0013	0.0201	6.4679	3.62	139.34 ± 2.41
1050	7.1744	0.0023	3.2176	0.0224	6.7504	7.21	145.19 ± 2.63
1100	6.6556	0.0009	1.8417	0.0209	6.5297	8.32	140.62 ± 1.70
1150	6.4471	0.0008	0.0013	0.0197	6.2044	12.63	133.86 ± 1.33
1200	6.4581	0.0009	3.1925	0.0188	6.4386	9.47	138.73 ± 1.98
1250	6.5960	0.0009	0.0013	0.0185	6.3248	5.48	136.37 ± 1.52
1400	8.2177	0.0042	0.0013	0.0191	6.9861	1.26	150.05 ± 4.11

References

Chang, E.Z., 1996. Collision orogene between north and south China and its eastern extension in the Korean Peninsula. Journal of Southeast Asian Earth Sciences 13, 267–277.

Chen, W.Q., Li, D.M., Li, Q., Wang, Q.L., 1989. Geochronological implications of K/Ar isotopic system of fault gouge: a preliminary study. Physics and Chemistry of Earth 17, 17–23.

Chen, J., Xie, Z., Liu, S., Li, X., Foland, K.A., 1995. Cooling age of Dabie orogen, China, determined by $^{40}Ar/^{39}Ar$ and fission track techniques. Science in China (series B) 38, 749–757.

Chung, S.L., 1999. Trace element and isotope characteristics of Cenozoic basalts around the Tanlu fault with implications for the eastern plate boundary between north and south China. The Journal of Geology 107, 301–312.

Dunlap, W.J., 1997. Neocrystallisation or cooling? $^{40}Ar/^{39}Ar$ ages of white mica from low-grade mylonites. Chemical Geology 143, 181–203.

Engebretson, D.C., Cox, A., Gorden, R.G., 1985. Relative motions between oceanic and continental plates in the Pacific basin. The Geological Society of America, Special Paper 206, 1–59.

Essene, E.J., 1989. The current status of thermobarometry in metamorphic rocks. In: Daly, J.S., Cliff, R.A., Yardley, B.W. (Eds.), Evolution of Metamorphic Belts. Geological Society Special Publication No. 43, pp. 1–44.

Faure, M., Lin, W., Scharer, U., Shu, L.S., Sun, Y., Arnaud, N., 2003. Continental subduction and exhumation of UHP tocks. Structural and geochronological insights from the Dabieshan (East China). Lithos 70, 213–241.

Gilder, S.A., Leloup, P.H., Courtillot, V., Chen, Y., Coe, R.S., Zhao, X., Xiao, W., Halim, N., Cogne, J.-P., Zhu, R., 1999. Tectonic evolution of the Tancheng–Lujiang (Tan–Lu) fault via middle Triassic to Early Cenozoic paleomagnetic data. Journal of Geophysical Research 104 (B7), 15365–15390.

Grimmer, J.C., Jonckheere, R., Enkelmann, E., Ratschbacher, L., Hacker, B.R., Blythe, A.E., Wagner, G.A., Wu, Q., Liu, S., Dong, S., 2002. Cretaceous–cenozoic history of the southern Tan–Lu fault zone: apatite fission-track and structural constraints from the Dabie Shan (eastern China). Tectonophysics 359, 225–253.

Hacker, B.R., Ratschbacher, L., Webb, L., McWilliams, M.O., Ireland, T., Calvert, A., Dong, S., Wenk, H-R., Chateigner, D., 2000. Exhumation of ultrahigh-pressure continental crust in east central China: Late Triassic-Early Jurassic tectonic unroofing. Journal of Geophysical Research 105 (B6), 13339–13364.

Harrison, T.M., 1981. Diffusion of ^{40}Ar in hornblende. Contributions to Mineralogy and Petrology 78, 324–331.

Harrison, T.M., Duncan, I., McDougall, I., 1985. Diffusion of ^{40}Ar in biotite: temperature, pressure and compositional effects. Geochimica et Cosmochimica Acta 49, 2461–2468.

Hong, J.P., Miyata, T., 1999. Strike-slip origin of Cretaceous Mazhan basin, the Tan–Lu fault zone, Shandong, East China. The Island Arc 8, 80–91.

Hsu, K.J., Li, J., Chen, I., Wang, Q., Sun, S., Sengor, A.M.C., 1987. Tectonic evolution of Qinling Mountains, China. Eclogae Geologicae Helvetiae 80, 735–752.

Li, R.W., Sang, H.Q., Zhang, R.H., Chu, Z.Y., Lin, S.Y., Jin, F.Q., Jiang, M.S., 2003. Geochronology of source materials from high-pressure and ultrahigh-pressure metamorphic rocks in Jurassic sedimentary rocks of Hefei Basin. Chinese Science Bulletin 48 (6), 605–610.

Li, S.G., Liu, D.L., Chen, Y.Z., Wang, S.S., Qiu, J., Hu, S.L., Sang, H.Q., 1993. Time of the blueschist belt formation in central China. Chinese Journal of Geology, 21–27 (in Chinese with English abstract).

Li, Z.X., 1994. Collision between the north and south blocks: a crust-detachment model for suturing in the region east of the Tan–Lu fault. Geology 22, 739–742.

Lin, A., Miyata, T., Wan, T.F., 1998. Tectonic characteristics of the central segment of the Tancheng–Lujiang fault zone, Shandong Peninsula, eastern China. Tectonophysics 293, 85–104.

Lin, J.L., Fuller, M., 1990. Paleomagnetism, North and South China collision, and the Tan–Lu fault. Philosophy Transaction of Royal Society of London A331, 589–598.

Lin, S., 1995. Collision between the North and South China blocks: a crustal-detachment model for suturing in the region east of the Tanlu fault: comment. Geology 23, 574–575.

Lin, S., 2001. $^{40}Ar/^{39}Ar$ age pattern associated with differential uplift along the Eastern highlands shear zone, cape Breton Island, Canadian Appalachians. Journal of Structural Geology 23, 1031–1042.

Ludwig, K.R., 2001. Isoplot—a geochronological toolkit for Microsoft Excel. Berkeley Geochronology Center Special Publication, No. 1a, 1–58.

Mancktelow, N.S., Pennacchioni, G., 2004. The influence of grain boundary fluids on the microstructure of quartz–feldspar mylonites. Journal of Structural Geology 26, 47–69.

Maruyama, S., Isozaki, Y., Kimura, G., Terabayashi, M.C., 1997. Paleogeographic maps of the Japanese Islands: plate tectonic synthesis from 750 Ma to the present. The Island Arc 6, 121–142.

Okay, A.I., Sengor, A.M.C., 1992. Evidence for intracontinental thrust related exhumation of the ultra-high-pressure rocks in China. Geology 20, 411–414.

Passchier, C.W., Trouw, R.A.J., 1996. Microtectonics. Springer, Berlin, pp. 48–95.

Ratschbacher, L., Hacker, B.R., Webb, L.E., McWilliams, M., Ireland, T., Dong, S.W., Calvert, A., Chateigner, D., 2000. Exhumation of the ultrahigh-pressure continental crust in east central China: Cretaceous and Cenozoic unroofing and the Tan–Lu fault zone. Journal of Geophysical Research 105 (B6), 13303–13338.

Reddy, .S.M., Potts, G.J., 1999. Constraining absolute deformation ages: the relationship between deformation mechanisms and isotope systematics. Journal of Structural Geology 21, 1255–1265.

Reddy, S.M., Kelley, S.P., Magennis, L.A., 1997. Microstructural and argon laserprobe study of shear zone development at the western margin of the Nanga Parbat–Haramosh Massif, western Himalaya. Contributions to Mineralogy and Petrology 128, 16–29.

Sibson, R.H., 1977. Fault rock and fault mechanism. Journal of Geological Society of London 133, 191–213.

Urai, J.L., Means, W.D., Lister, G.S., 1986. Dynamic recrystallization of minerals. In: Hobbs, B.E., Heard, H.C. (Eds.), Mineral and rock Deformation: Laboratory studies. The Paterson Volume. Geophysical Monograph 36. American Geophysical Union, Washington, DC, pp. 161–199.

Wan, T.F., Zhu, H., 1996. The maximum sinistral strike-slip displacement and formation time of the Tan–Lu fault zone. Geological Journal of China Universities 2, 14–27 (in Chinese with English abstract).

Wang, X.F., Li, Z.J., Chen, B.L., Zhang, Q., Chen, X.H., Xin, L.S., Chen, Z.L., Dong, S.W., Wu, H.M., 1998. Formation and evolution of the Tan–Lu strike-slip fault system and its geological significance. In: Zheng, Y.Z. (Ed.), Proceedings of 30th International Geological Congress. Geological Publishing House, Beijing, pp. 176–196 (in Chinese).

Xu, J.W., Zhu, G., 1994. Tectonic models of the Tan–Lu fault zone, eastern China. International Geology Review 36, 771–784.

Xu, J.W., Zhu, G., Tong, W.X., Cui, K.R., Liu, Q., 1987. Formation and evolution of the Tancheng–Lujiang wrench fault system: a major shear system to the northern of the Pacific Ocean. Tectonophysics 134, 273–310.

Xu, J.W., Ma, G.F., Tong, W.X., Zhu, G., Lin, S.F., 1993. Displacement of the Tancheng–Lujiang wrench fault system and its geodynamic setting in the northwestern circum-Pacific. In: Xu, J.W. (Ed.), The Tancheng–Lujiang Wrench Fault System. Wiley, Chichester, UK, pp. 51–76.

Yin, A., Nie, S.Y., 1993. An indentation model for the North and South China collision and the development of the Tan–Lu and Honam fault system, eastern Asia. Tectonics 12, 801–813.

Zhang, K.J., 1997. North and South China collision along the eastern and southern North China margins. Tectonophysics 270, 145–156.

Zhang, Y.Q., Dong, S.W., Shi, W., 2003. Cretaceous deformation history of the middle Tan–Lu fault zone in Shandong Province, eastern China. Tectonophysics 363, 243–258.

Zhang, Y.Q., Chen, W., Yang, N., 2004. $^{40}Ar/^{39}Ar$ dating of shear deformation of the Xianshuihe fault zone in west Sichuan and its tectonic significance. Science in China (Series D) 9, 794–803.

Zhang, Zh. M., Liou, J.G., Coleman, R.G., 1984. An outline of the plate tectonics of China. Geological Society of America Bulletin 95, 295–312.

Zhou, J.P., Miyata, T., Wang, L., 1999. An early Cretaceous pull-part basin in the middle section of the Tan–Lu fault zone. Seismological Geology, 185–192 (in Chinese with English abstract).

Zhou, X.M., Li, X.W., 2000. Origin of late Mesozoic igneous rocks in Southeastern China: implications for lithosphere subduction and underplating of mafic magmas. Tectonophysics 326, 269–287.

Zhu, G., Xu, J.W., 1997. Displacement, timing and tectonic model of the Tan–Lu fault zone. In: Zheng, Y.Z. (Ed.), Proceedings of 30th International Geological Congress, 14. VSP, Holland, pp. 217–228.

Zhu, G., Xu, J.W., Shun, S.J., 1995. Isotopic age evidence for the timing of strike-slip movement of the Tan–Lu fault zone. Geological Review 41 (5), 452–461 (in Chinese with English abstract).

Zhu, G., Song, C.Z., Wang, D.X., Liu, G.S., Xu, J.W., 2001a. Studies on $^{40}Ar/^{39}Ar$ thermochronology of strike-slip time of the Tan–Lu fault zone and their tectonic implications. Science in China (Series D) 44, 1002–1009.

Zhu, G., Wang, D.X., Liu, G.S., Song, C.Z., Xu, J.W., Niu, M.L., 2001b. Extensional activities along the Tan–Lu fault and its geodynamic setting. Chinese Journal of Geology 36, 269–278 (in Chinese with English abstract).

Zhu, G., Wang, D.X., Liu, G.S., Niu, M.L., Song, C.Z., 2004. Evolution of the Tan–Lu fault zone and its response to plate movements in West Pacific basin. Chinese Journal of Geology 39, 36–49 (in Chinese with English abstract).